Neuronal arithmetic

R. Angus Silver

Abstract | The vast computational power of the brain has traditionally been viewed as arising from the complex connectivity of neural networks, in which an individual neuron acts as a simple linear summation and thresholding device. However, recent studies show that individual neurons utilize a wealth of nonlinear mechanisms to transform synaptic input into output firing. These mechanisms can arise from synaptic plasticity, synaptic noise, and somatic and dendritic conductances. This tool kit of nonlinear mechanisms confers considerable computational power on both morphologically simple and more complex neurons, enabling them to perform a range of arithmetic operations on signals encoded in a variety of different ways.

Multiplying two numbers together in your head is a difficult task if you did not learn multiplication tables as a child. On the face of it, this is somewhat surprising given the remarkable power of the brain to perform complex computational tasks, such as coordinating limbs, balancing and calculating object trajectories when playing a game of tennis. Traditionally, it was thought that each individual neuron could only perform a weighted sum of its synaptic inputs (a linear operation) followed by a nonlinear thresholding operation (all-or-none response) and that even low level computations, such as multiplication of signals, had to be carried out by groups of neurons[1]. Subsequent theoretical work suggested that single neurons could act as more powerful computational units[2–8], and this view has now been strengthened by a considerable body of experimental work, which shows that even the most humble of the brain's 10^{11} neurons[9] can rapidly perform both sums and multiplications on their synaptic inputs. The main focus of this Review will be to discuss the various biophysical mechanisms that enable an individual neuron to rapidly perform arithmetic operations on the signals it receives through its synaptic inputs, thereby allowing information to be transformed and combined before it is converted into neuronal output. The mechanisms involved will be discussed in relation to neuronal morphology and the way in which information is represented, as this allows identification of the cell types and the neural coding regimes in which they are likely to operate.

Department of Neuroscience, Physiology and Pharmacology, University College London, Gower Street, London WC1E 6BT, UK.
e-mail:
a.silver@ucl.ac.uk
doi:10.1038/nrn2864
Published online 9 June 2010

Encoding information with action potentials

Information can be represented in a number of different ways by neural activity, but neural coding is often cast in one of two extremes: either as a firing rate or as correlations in spike timing. The pioneering work of Adrian and Zotterman[10,11] established that continuous sensory variables such as touch, pressure and muscle load can be encoded in the rate of sustained action potential (AP) firing. Recent intracellular recordings from cerebellar granule cells (CGCs) *in vivo* show that rate-coded vestibular inputs that signal head velocity are linearly encoded at input synapses through the bidirectional modulation of the excitatory postsynaptic current frequency and postsynaptic charge[12]. The way in which such a neuron integrates this sustained excitatory rate-coded synaptic input and transforms it into output firing can be simply captured by its input–output (I–O) relationship (FIG. 1a,b). By contrast, *in vivo* recordings from several areas of the neocortex suggest that only a small fraction of neurons in a network spike in response to a particular sensory stimulus[13–17]. Under these sparse coding[13,14] conditions the mean firing rate of individual neurons is often less than 1 Hz[15–17] and coding can involve as little as a single spike per neuron[18]. Sparse population coding is a compromise between the extremes of local codes, in which each neuron in the network represents a single feature or concept, and dense holographic codes[19] in which each feature is represented in all cells, allowing the storage of many more features than there are neurons in the network. Moreover, theory predicts that the most energy-efficient codes for representing information are sparse, as observed experimentally[20,21]. Under sparse coding regimes the neuron acts as a coincidence detector of temporally correlated inputs, rather than as an integrator. The I–O relationship can be defined as the relationship between spike probability and the number of coincident inputs (P_{spike}–N_{exc}; FIG. 2a–c) or, in the temporal domain, as the standard deviation of input spike times (P_{spike}–σ_{input}; FIG. 2d,e).

This has the advantage that it directly represents how synaptic inputs with different temporal correlations are transformed by the neuron. Synaptic integration during sparse neural activity, when the interval between spikes is long, is distinct from that for sustained high frequency firing regimes, when the AP and ensuing afterhyperpolarizing (AHP) conductances can dominate the electrical behaviour of the cell[22,23]. Differences in the frequency of firing and the way in which information is encoded are therefore important for understanding the neuronal I–O relationship, the computations performed by a single neuron and the biophysical mechanisms involved.

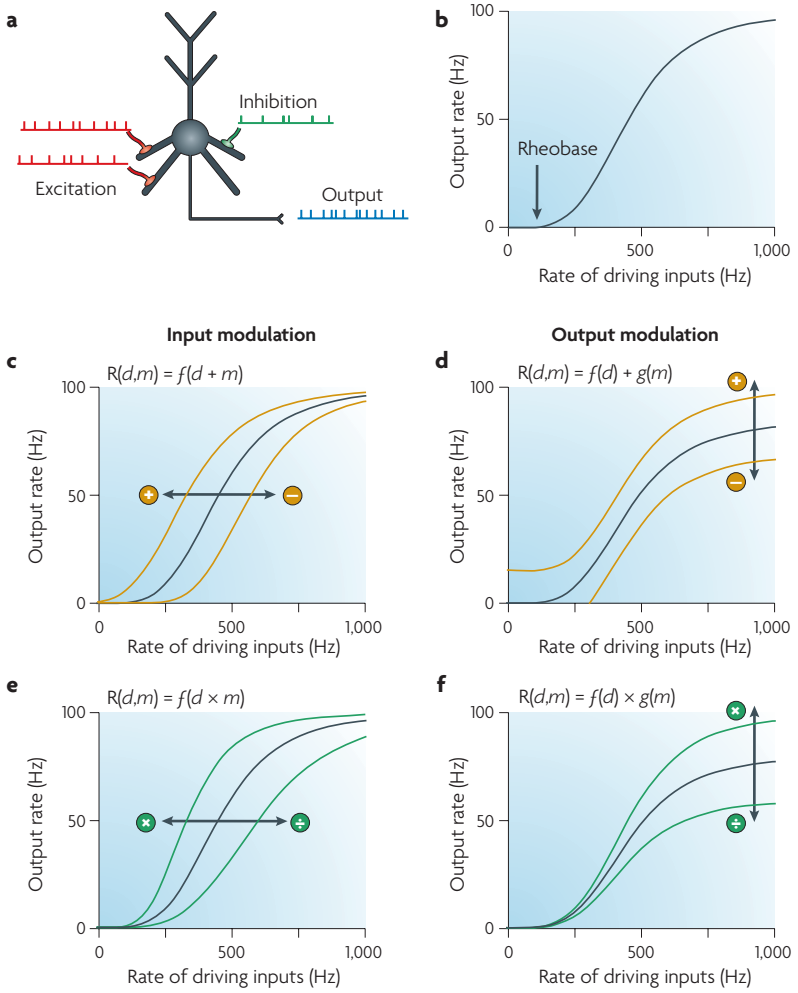

Figure 1 | **The rate-coded neuronal input–output relationship and possible arithmetic operations performed by modulatory inputs. a** | For rate-coded neuronal signalling, a driving input typically consists of asynchronous excitatory synaptic input from multiple presynaptic neurons firing in a sustained manner (shown in red). A neuron may also receive a modulatory input, such as inhibition (shown in green), that alters the way the neuron transforms its synaptic input into output firing rate (shown in blue). **b** | The input–output (I–O) relationship between the total (or mean) driving input rate (*d*) and the response that is represented by the output firing rate (R). The arrow indicates the rheobase (minimum synaptic input that generates an action potential). **c** | Rate-coded I–O relationships can be altered by changing the strength of the modulatory input (*m*), which may be mediated by a different inhibitory or excitatory input. If this shifts the I–O relationship along the *x*-axis to the right or left, changing the rheobase but not the shape of the curve, an additive operation has been performed on the input (shown by orange curves). This input modulation is often referred to as linear integration because the synaptic inputs are being summed. **d** | An additive operation can also be performed on output firing. In this case a modulatory input shifts the I–O relationship up or down along the *y*-axis (shown by orange curves). **e**,**f** | If the driving and modulatory inputs are multiplied together by the neuron, changing the strength of a modulatory input will change the slope, or gain, of the I–O relationship without changing the rheobase. A multiplicative operation can produce a scaling of the I–O relationship along either the *x*-axis (input modulation; **e**) or the *y*-axis (output modulation; **f**). Although both of these modulations change the gain of the I–O relationship, only output gain modulation scales the neuronal dynamic range (**f**).

Algebraic transformation of I–O relationships

In this section we will use rate-coded signals to illustrate how a group of synaptic inputs can rapidly alter the shape of a neuron's I–O relationship in ways that correspond to arithmetic operations (FIG. 1). These inputs are often referred to as modulatory inputs to distinguish them from the driving inputs. Modulatory inputs can be excitatory synaptic inputs that convey a different signal to the driving inputs, inhibitory inputs, or slow changes in neural excitability arising from neuromodulatory substances such as acetylcholine and serotonin[24]. However, only rapid synaptic modulations are considered in this article.

Additive operations. The response R of a neuron when a driving input *d* and a modulatory input *m* are added, can be defined in two different ways. When a modulatory input is added to the driving input and then transformed through the spiking mechanism the operation can be written as $R(d,m) = f(d + m)$. This shifts the I–O relationship along the input, or *x*-axis, with a leftward shift corresponding to addition and a rightward shift corresponding to subtraction (FIG. 1c). This type of linear additive modulation has been observed when the modulatory input is a fixed current or conductance[22]. When the modulatory input is independent of the I–O relationship of the driving input, the neuronal response can be defined as $R(d,m) = f(d) + g(m)$. In this case, a modulatory input shifts the I–O relationship along the output or *y*-axis (FIG. 1d), the simplest example being a change in the basal firing rate of the neuron in the absence of an excitatory drive.

Multiplicative operations. Muliplication of driving and modulatory inputs can also be defined in two ways. $R(d,m) = f(d \times m)$ defines multiplicative input modulation (FIG. 1e) and $R(d,m) = f(d) \times g(m)$ defines output modulation (FIG. 1f). In both cases multiplication by a constant produces a change in the slope of the rate-coded I–O relationship, also referred to as a change in neuronal gain[25]. An increase in neuronal gain corresponds to a multiplication and a decrease corresponds to a division. A change in gain alters the sensitivity of a neuron to changes in its driving inputs without affecting its selectivity or receptive field properties[26]. For input gain modulation, the maximum value of the I–O relationship is not changed following the modulation, but for output gain modulation, the maximum firing rate is scaled up or down (FIG. 1e,f). The multiplicative and additive operations that are performed by neurons can be separated and quantified by fitting their I–O relationships with empirical functions before and after modulation (Supplementary information S1 (box)).

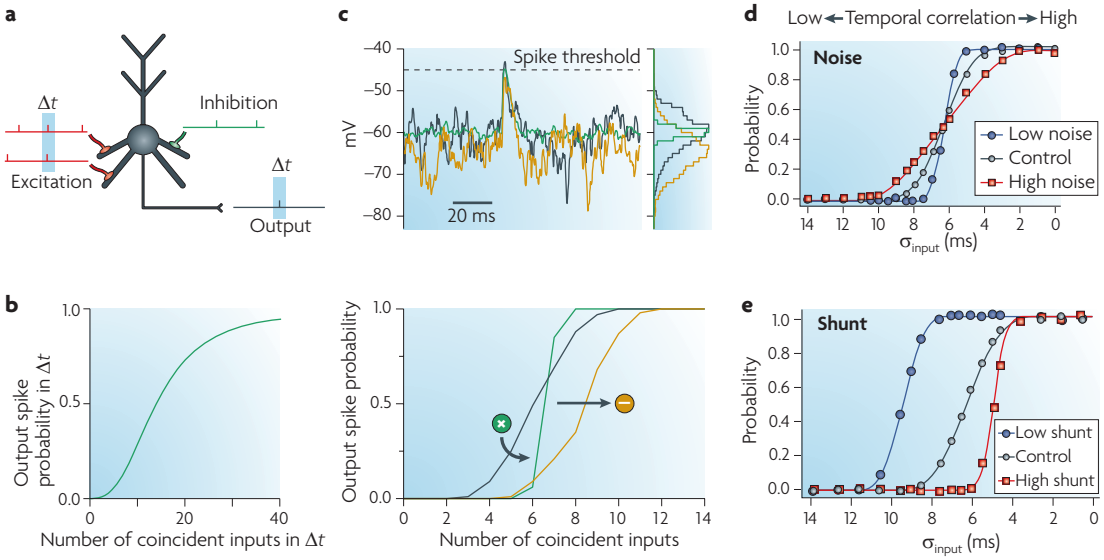

Figure 2 | **Neuronal arithmetic during sparse coding. a** | Sparse coding relies on coincident synaptic input within a brief time-window (Δt) during which the inputs are integrated and potentially drive the cell to cross the action potential threshold. **b** | Spike probability versus the number of coincident driving inputs (P_{spike}–N_{exc}) is the simplest way to quantify the neuron's input–output (I–O) relationship under these conditions. **c** | Background synaptic noise is important in determining the shape of the P_{spike}–N_{exc} relationship[73,76] because it determines the width of the membrane voltage distribution. The simulation shows a simple integrate-and-fire cell with background voltage noise, driven with a synchronous synaptic input (top part). Shifting the voltage distribution without changing its shape by adding a hyperpolarizing current introduces a subtractive shift in the P_{spike}–N_{exc} relationship (bottom part; shift from black to orange traces). By contrast, decreasing the voltage noise increases the gain of the I–O relationship (shift from black to green traces). **d** | The relationship between P_{spike} and driving inputs can also be defined in the temporal domain. In this case, the temporal correlation in the driving inputs is defined as the standard deviation of input spike times (σ_{input})[48,50]. Altering the level of noise changes the gain of the P_{spike}–σ_{input} relationship[47,48]. **e** | Changing the input resistance by altering a shunting conductance tends to shift the P_{spike}–σ_{input} relationship[48]. This is due to scaling of the excitatory postsynaptic potential (EPSP) and voltage noise, together with altered summation of temporally dispersed inputs, as a result of changes in membrane time constant and thus EPSP shape (FIG. 3a). Parts **d** and **e** are modified, with permission, from REF. 48 © (2005) The American Physiological Society.

Role of arithmetic operations *in vivo*

Additive operations. Additive operations can enable a neuron to perform the same rate-coded I–O operation under conditions of different excitatory or inhibitory drive. However, additive operations also alter the number of inputs required to reach threshold, which may change population sparseness and the ability to distinguish different patterns of activation. In the temporal domain, additive operations can potentially alter the range of temporal correlations in the synaptic input to which the neuron responds (FIG. 2e). Additive changes in the rate-coded I–O relationship were observed in motor neurons *in vivo*, when synaptic input was stimulated on different dendritic branches[27] and when the I–O relationship was assayed with current injections[28]. Additive operations can also underlie sophisticated sensory processing — for example, theoretical[29] and experimental[30] studies suggest that populations of neurons can represent uncertainty in sensory variables and that additive operations are important for computing with these probabilistic population codes[29]. Although such examples show that additive operations are important for signal processing, many neuronal computations are thought to require a multiplicative operation.

Multiplicative operations. Simple multiplicative operations in neuronal systems are important for signal amplification, normalization and preventing saturation of firing (FIG. 1e,f), allowing efficient information transmission[31]. Multiplicative operations occur *in vivo* in a wide range of sensory systems. In the monkey parietal cortex, visual responses of neurons are multiplicatively scaled by eye position[32,33] and head position[34]. These and other observations are complemented by several theoretical studies that have shown that multiplication of sensory signals is essential for the coordinate transforms that are required for visually guided reaching[35–37]. Related computations are also found in the vestibular cerebellum, in which head-centered vestibular afferent information is transformed into earth-referenced self motion[38]. Indeed, gain modulation is widespread[26]: it occurs during attentional scaling of orientation tuning curves[39], of direction tuning curves[40] and of translation-invariant object recognition[41], with contrast invariance of orientation tuning[42] and during auditory processing[43]. These studies show that the brain uses multiplicative operations in a wide range of tasks.

Changing the gain of subsets of neurons in a synaptically coupled network will alter the functional connectivity and thus the dynamic pattern of neuronal activation. This

Neuronal gain
The slope of the neuronal input–output relationship. Changing the neuronal gain alters the sensitivity of a neuron to changes in driving inputs.

Coordinate transform
The conversion of one coordinate system to another — for example, the brain converts visual information from retina-centric to body-centric coordinates, taking account of gaze angle during visually guided reaching.

Driving force
The difference between the membrane potential and the reversal potential of an ionic conductance.

Membrane time constant
The product of the capacitance and resistance of the cell membrane, characterizing how rapidly a current changes the membrane potential. The smaller the time constant the faster the membrane potential can change.

realization has lead to the proposal that gain modulation controls the selection of different neuronal assemblies used for distinct computational tasks[44–46]. For neurons operating in coincidence-detection mode under sparse activation conditions, the gain of the I–O relationship also determines the shape of the time-window in which inputs can be integrated to generate a spike, with higher gain giving a sharper cut-off (FIG. 2d). Thus, through such arithmetic operations an individual neuron can potentially control both the width and 'roll-off' of the temporal correlation window for synaptic integration[47,48] and hence also control the temporal properties of signals that can propagate through the network[49,50].

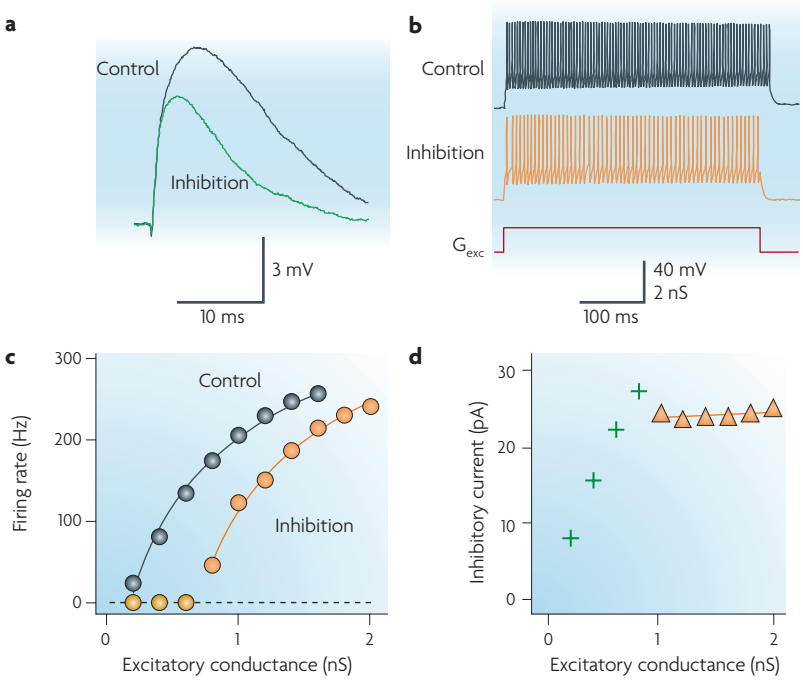

Figure 3 | **Subthreshold effects of shunting conductance and its effect on the input–output relationship of a cerebellar granule cell in the absence of noise.** The effect of shunting inhibition on cerebellar granule cells (CGCs) was investigated in acute cerebellar slices using the dynamic clamp technique. **a** | An excitatory postsynaptic potential (EPSP) evoked by an AMPAR (α-amino-3-hydroxy-5-methyl-4-isoxazole propionic acid receptor) synaptic conductance waveform (reversal potential 0 mV) that was injected during control conditions (shown in black) and during application of a 1 nanosiemens (nS) tonic shunting inhibitory conductance (reversal potential –75 mV). This inhibitory conductance scaled down the amplitude of the EPSP, consistent with Ohm's law, and accelerated the decay of the EPSP as a result of a reduction in the membrane time constant (shown in green). **b** | CGC firing responses to a noise-free excitatory conductance step (G_{exc}, shown in red). The upper traces show the voltage responses to G_{exc} under control conditions (shown in black) and during injection of an inhibitory conductance (shown in orange). **c** | The relationship between mean firing rate of a CGC and step excitatory conductance in the presence and absence (control) of an inhibitory conductance. The inhibitory conductance produced a purely subtractive input modulation (*x*-axis shift; FIG. 1c) in the neuronal input–output relationship. **d** | The relationship between current flow through the tonic inhibitory conductance and the driving excitatory conductance, for subthreshold voltages (+) and during spiking (Δ). The inhibitory current depends on the excitatory conductance as the subthreshold voltage depolarizes, as expected for a conductance. However, during sustained firing the shunting inhibitory conductance behaves like a constant current source[22]. This explains why shunting inhibition has a multiplicative effect on subthreshold inputs but has an additive effect during sustained firing under low noise conditions. Figure is modified, with permission, from REF. 23 © (2003) Elsevier.

Mechanisms underlying arithmetic operations

Subthreshold synaptic integration and linear operations. The way in which synaptic inputs are combined is largely determined by the electrical properties of the membrane. The membrane potential of a neuron increases from its resting membrane potential (typically –75 mV) during excitatory synaptic input, when current flows into the cell through transient conductances at each of the activated synapses. The resulting excitatory postsynaptic potentials (EPSPs) do not sum linearly with increasing numbers of active synapses because current flow through a synaptic conductance depends on the driving force, which is reduced as the voltage increases. Increasing synaptic conductance also lowers the resistance of the cell membrane and this reduces both the change in voltage produced by a current and the membrane time constant. Increasing membrane conductance in electrically compact neurons, such as the CGCs, therefore scales down the amplitude and speeds the decay of EPSPs (FIG. 3a). Although these synaptic conductance effects also occur locally in the dendrites of morphologically complex cells, such as cortical pyramidal cells, brief conductances arising from distant dendritic synapses may have little effect on each other or on the somatic input resistance because the space constant for conductance is half of that for voltage[51,52]. Their effect on the soma is therefore more like a group of current sources that add linearly. These passive subthreshold mechanisms contribute to the linearizing integration of EPSPs distributed on dendritic trees.

Shunting inhibitory conductances. Inhibitory synapses are often located close to the soma, where their conductance can have a large effect on somatic input resistance[5,52–54] (and thus spiking) because of the proximity to the spike initiation zone. Fast inhibitory transmission is typically mediated by $GABA_A$ (γ-aminobutyric acid type A) receptors, which conduct Cl^- and HCO_3^- ions and often have a reversal potential close to the resting potential. At resting potential, little current is generated by these synapses due to the small driving force, but the increase in membrane conductance that they introduce short-circuits excitatory synaptic currents by locally reducing the input resistance. These shunting inhibitory conductances (also known as silent inhibitory conductances), which can be strong *in vivo*[54], scale down EPSPs in a multiplicative manner (FIG. 3a), in accordance with Ohm's law, as recognized many years ago[55,56]. Classical theoretical work suggests that the arithmetic operations resulting from shunting inhibition depend on the size and location of the conductance; inhibition may have a divisive effect on the EPSP if the conductance is large and located close to the soma, but may have a subtractive effect if the conductance is small and spatially distributed[2,57]. Inhibitory synapses placed between a distal excitatory input and the soma are effective, especially when located close together[2,4,5,8,27]. This may enable dendritic-branch-specific veto and logical AND–NOT operations[4], a conclusion that has been strengthened by more recent experimental work[58]. Together, these studies of subthreshold interactions of coincident excitatory and inhibitory postsynaptic conductances

suggested that individual neurons could perform a variety of multiplicative and logical operations. This led to the proposal that shunting inhibition mediates the divisive gain modulation required in models of visual cortex to account for neural responses to drifting gratings at different contrast and orientations[59] and for gain modulation in electric fish[60].

Surprisingly, subsequent work with biologically realistic neuronal models predicted that shunting inhibition has a subtractive rather than a divisive effect on sustained rate-coded I–O relationships[22,61,62]. We illustrate this with experiments on CGCs (FIG. 3b,c). During sustained firing the voltage is clamped close to the spike threshold voltage by the powerful potassium conductances that underlie AP repolarization and spike AHP[63]. This converts the steady shunting conductance into a current source[22,23] (FIG. 3d), which shifts the relationship between output firing and driving current[28,64–67] or input conductance[23], along the input axis in a purely subtractive manner (FIG. 3c). These findings implied that multiplicative interactions between conductances (discussed above for subtheshold integration) did not hold for sustained rate-coded signalling. However, an important factor had been overlooked in the study of neuronal gain; *in vivo* recordings showed that neurons are often bombarded by synaptic conductances, and this produces high levels of stochastic voltage noise and lowers the input resistance[54,68,69] (FIG. 4a), a condition not typically present in *in vitro* slice preparations in which long-range synaptic connections are cut. The presence of synaptic noise has important implications for neuronal computation for both sustained rate-coded and sparse temporal signalling, as discussed in the next section.

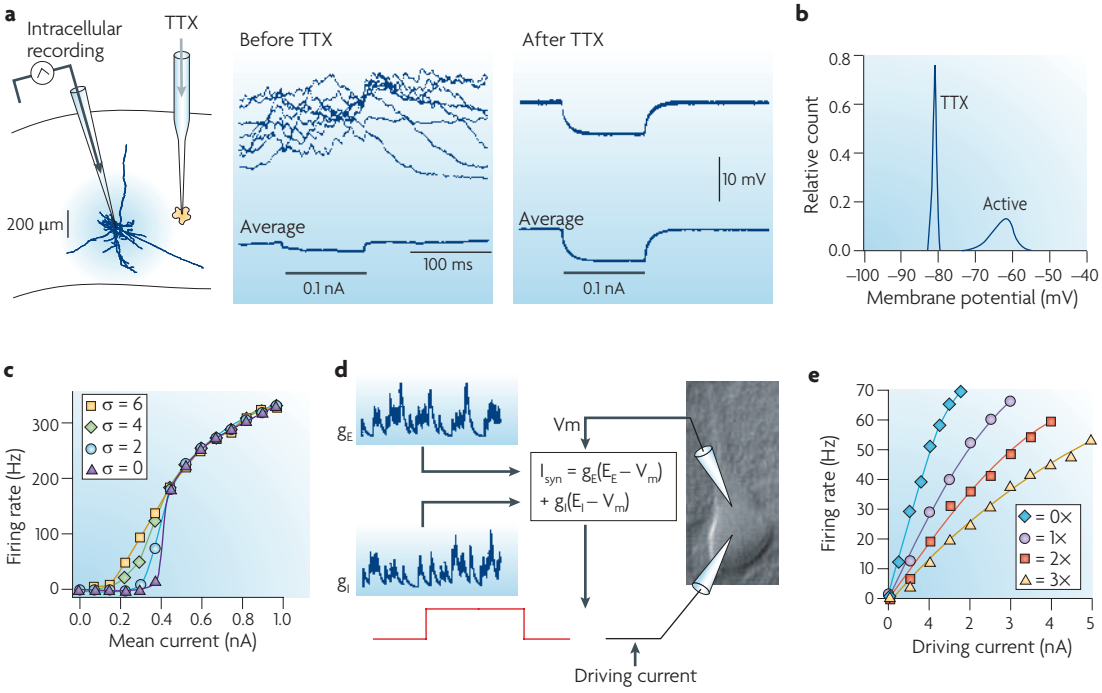

Figure 4 | **Synaptic voltage noise and gain modulation of the rate-coded input–output relationship. a** | Schematic setup for intracellular voltage recordings from a neocortical pyramidal neuron in a cat under anaesthesia. The intracellular voltage is characterized by a high level of noise in each recording period. Blocking synaptic input with local injection of tetrodotoxin (TTX), eliminated the voltage noise and increased the input resistance of the cell (see the voltage response to a current step of 0.1 nanoamperes (nA)). **b** | Blocking synaptic input with TTX reduces the variance of the intracellular voltage distribution in pyramidal neurons and demonstrates that some cortical cells operate under conditions of high levels of synaptically induced voltage noise (active) *in vivo*. **c** | The effect of noise on the relationship between firing rate and current (F–I) for a cortical interneuron, recorded in an acute slice preparation. As the noise increases (σ indicates standard deviation of the voltage noise in mV), the foot of the F–I relationship becomes more pronounced, reducing the gain of the relationship and producing a more sigmoid shape. **d** | The dynamic clamp configuration used to inject balanced excitatory (g_E) and inhibitory (g_I) synaptic conductance trains (resulting in zero net excitatory drive) into neocortical pyramidal cells, mimicking background synaptic input (noise) in the acute slice. Current steps were used as driving inputs to assay the neuronal responsiveness. I_{syn} is the synaptic current and E_E and E_I are the excitatory and inhibitory reversal potentials, respectively. **e** | The relationship between firing rate and the amplitude of the driving current steps for different levels of synaptic conductance noise (multiples of X, a balance of excitatory (rate = 7,000 Hz) and inhibitory synaptic inputs (rate = 3,000 Hz)). As the level of noise increases the gain of the F–I relationship was modified in a divisive manner. Part **a** is modified, with permission, from *Nature Reviews Neuroscience* REF. 69 © (2003) Macmillan Publishers Ltd. All rights reserved. Part **b** is modified, with permission, from REF. 68 © (1999) The American Physiological Society. Part **c** is modified, with permission, from REF. 80 © (2006) Society for Neuroscience. Parts **d** and **e** are modified, with permission, from REF. 66 © (2002) Elsevier.

Space constant
The distance over which a voltage imposed at a point will have decreased to 1/e (Euler's number) (~37%) of its original value; a measure of how far a subthreshold potential will spread along an axon or dendrite. The thinner the dendritic branch, the shorter its space constant.

Reversal potential
The potential at which the electrochemical gradient is zero and there is no net current flow though a conductance.

Shunting inhibitory conductance
(Also known as silent inhibitory conductance.) An inhibitory conductance that reduces the depolarization produced by an excitatory current by increasing membrane conductance.

Ohm's law
The current across a conductor is linearly proportional to the potential difference (voltage).

AND–NOT operation
A logical operation in which an output only occurs when one input is on and the other is off.

Drifting gratings
A visual stimulus that consists of alternating black and white bars that drift in a particular direction.

The role of changes in noise and conductance

Synaptic noise. Stochastic noise arising from synaptic conductances produces voltage fluctuations, converting a relatively constant subthreshold voltage into a distribution of values (FIG. 4a,b). When investigators began to include physiologically relevant levels of synaptic noise in their simulations and *in vitro* experiments, they found that the shape of the I–O relationships for both sparse coincident[48,70–76] and sustained rate-coded[23,42,66,77–82] inputs were fundamentally altered. This occurs because voltage fluctuations enable synaptic inputs to cross the threshold and trigger a spike even when the mean voltage is well below the spike threshold, thereby extending the range of excitation over which a neuron can signal. This shifts the rheobase of the neuronal I–O relationship and decreases the slope or gain of both the P_{spike}–N_{exc} and the P_{spike}–σ_{input} relationships driven by sparse coincident input[48,73,74] (FIG. 2c,d). This broadens the synaptic input correlation window that the neuron can respond to (FIG. 2d). Noise has similar effects on the shape of the rate-coded I–O relationship. The leftward additive shift was more pronounced when currents were used to drive the cell[80] (FIG. 4c) or in simulations[78] than when conductance noise was used (FIG. 4d,e). This is because the leftward shift in the rate-coded I–O was counteracted by a rightward shift introduced by the shunting effect of the input conductance[66,78]. These results show that changing the level of noise is a powerful way to change neuronal gain irrespective of the coding regime.

Background noise induced by balanced background synaptic input. For neurons, such as pyramidal neurons, that require a large number of synaptic inputs to reach threshold, high levels of voltage noise can only be achieved during uncorrelated (asynchronous) rate-coded inputs when excitatory and inhibitory synaptic conductances are balanced. Under these conditions high rates of synaptic conductance can be applied without a net excitatory or inhibitory effect. Introducing such a noisy conductance input using the dynamic clamp in combination with excitation through a noise-free driving current step (FIG. 4d) allows the level of noise and conductance to be altered independently of the excitatory drive[66]. When excitatory and inhibitory conductances were balanced, the leftward shift in the I–O relationship caused by increasing noise was counteracted by the rightward shift caused by reduced input resistance, leaving a purely multiplicative gain change and no additive shift[66] (FIG. 4e). For this to occur *in vivo*, a suitably tuned network architecture that supports precisely balanced excitation and inhibition, would be required. Feedforward and feedback connections in cortical circuits may achieve such balance if coupled with inhibitory cells that compensate for their low numbers with higher sensitivity, firing rate and synaptic conductances[83–85]. However, the effect on neuronal gain of increasing the level of noise is not always so clean-cut; depending on the cell type and the nature of the interactions of noise with Na^+ and various AHP conductances[80,86], neuronal gain can either increase or decrease. Nevertheless, these studies are consistent with the idea that changes in the level of input noise cause gain modulation.

The effect of conductance in the presence of synaptic noise. Dynamic clamp experiments and modelling show that hyperpolarization and increases in somatic membrane conductance introduce subtractive shifts in the P_{spike}–N_{exc} relationship[70,73,74,76]. Hyperpolarization performs a subtractive operation because additional excitation is required to reach the original rheobase voltage, and voltage noise and thus gain are unaltered (FIG. 2c). For changes in somatic input resistance, which occur during shunting inhibition, the EPSP amplitude and voltage fluctuations are likely to be scaled down equally, leaving the gain of the P_{spike}–N_{exc} relationship unchanged[73]. Moreover, nonlinear shunting conductances can help to linearize such subtractive shifts in the P_{spike}–N_{exc} relationship[87]. These studies show that in the presence of background noise, adding a hyperpolarizing current or increasing shunting inhibition has a subtractive effect and this narrows the input correlation window to which the neuron responds (FIG. 2e). Experiments on sustained rate-coded I–O relationships also suggested that shunting inhibition has a purely subtractive effect when the level of synaptic input noise is fixed[23,66,87].

This view that conductance always has a subtractive effect on I–O relationships seems to be at odds with theoretical and experimental studies that show that simply applying an inhibitory conductance can alter neuronal gain[23,77,79,88]. Indeed, applying a fixed tonic inhibitory conductance produced a robust gain change in the I–O relationship of CGCs when they were driven with synaptic-like rate-coded excitatory conductances delivered with the dynamic clamp technique[23] (FIG. 5a,b). This was not a nonlinear dendritic effect because CGCs are among the smallest and simplest neurons in the brain and ideally suited to the dynamic clamp technique, as their soma and dendrites form a single electrical compartment[89,90]. The resolution of these apparently contradictory effects of conductance on the I–O relationship lay in the fact that the variance of rate-coded synaptic conductance trains increases with the mean rate according to Campbell's theorem[23,77,91] (FIG. 5c). Rate-coded inputs therefore introduce a frequency-dependent increase in noise, which when combined with a shunting conductance produces a gain change without requiring an externally driven change in background noise or a balanced synaptic input[23]. However, without balanced excitation and inhibition, a subtractive component is also present (FIG. 5b). This conductance-mediated gain modulation is particularly effective for small cells — such as CGCs — with rapid synaptic conductances that require few driving inputs to reach threshold, because these produce high levels of voltage noise during rate-coded excitation[23]. In larger neurons, such as pyramidal cells, the voltage noise generated by excitatory input alone is relatively small when inputs are asynchronous and thus the effect of conductance is largely additive under these conditions.

Rheobase
The minimum current or conductance that produces an action potential in a neuron.

Dynamic clamp
An electrode-based electrophysiological device that uses an electrical circuit or computer simulation to inject artificial conductances into a neuron.

Campbell's theorem
A mathematical theorem that describes the relationship between the frequency of brief, randomly occurring, exponentially decaying events and the time-averaged value of their mean and the variance.

Power law
A mathematical relationship between two quantities (for example, x and y) of the form $y(x) = kx^n$, in which k is a constant and n is the exponent. Such relationships have the special property that they are scale invariant.

Whether a shunting inhibitory conductance can modulate rate-coded neuronal gain in the presence of a fixed level of noise has also been a matter of debate. Experimental and theoretical work suggests that conductance does not change neuronal gain in the presence of fixed noise[66,92]. However, simulations predict that modest gain changes can occur under some conditions[23,79]. Although such gain changes are weaker than those for variable noise and only occur for small modulatory inputs and relatively low firing rates, the mechanism underlying this effect provides insights into the mechanisms of noise- and conductance-based gain modulation. Noise converts the relationship between output firing rate and mean voltage f_{out}–V_m from a step-like threshold to a smooth function that approximates a power law[23,42,79,81,82,93] (FIG. 5d). Changes in subthreshold voltage caused by a modulatory input can be coupled to output spiking through this continuous function. The shape of the f_{out}–V_m relationship is important as power laws can perform a crude form of multiplication[81], because additive shifts along the x-axis can have a multiplicative action as a function of the x-axis (Supplementary information S1 (box)). However, for modulatory inputs to produce changes in gain without an additive shift[66] or for these gain changes to be a function of both the x- and y-axes, an additional nonlinearity[93] or a change in the f_{out}–V_m relationship is required (R.A.S. and V. Steuber, unpublished observations). Indeed, changes in the exponent of the power law are expected if the level of synaptic noise changes[66], if the frequency of rate-coded excitatory input is altered[23] or if the rate of an inhibitory synaptic input is modified[77,79,88]. All of these changes produce a robust gain change as a function of both the x- and y-axes. Thus, synaptic noise enables shunting inhibition to modulate neuronal gain during sustained firing, thereby providing a biologically plausible mechanism for those early models that proposed that shunting inhibition performs gain modulation[59,60]. However, this does not generalize to temporally correlated signalling, where it is subtractive[73] .

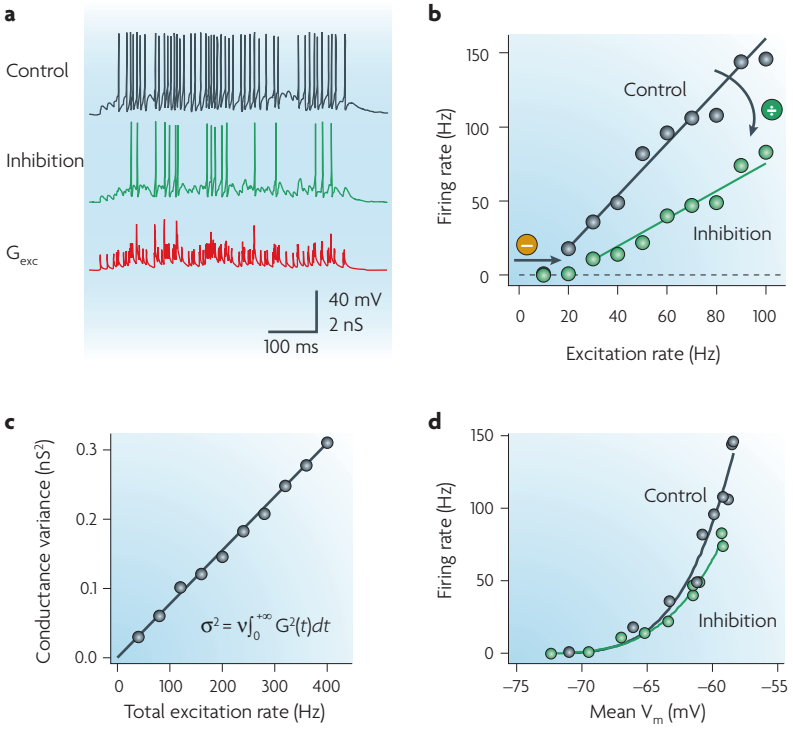

Figure 5 | **Inhibition-mediated gain modulation with noisy rate-coded synaptic input in cerebellar granule cells.** The effect of shunting inhibition on the rate coded input-output (I–O) relationship of cerebellar granule cells (CGCs) driven with random trains of noisy, synaptic-like conductances in the acute cerebellar slice preparation using the dynamic clamp technique. **a** | A CGC was excited by four summed Poisson trains of AMPAR (α-amino-3-hydroxy-5-methyl-4-isoxazole propionic acid receptor) synaptic conductances (G_{exc}) with a reversal potential of 0 mV under control conditions and during a 1 nanosiemens (nS) constant (tonic) inhibitory conductance. The resulting relationships between CGC firing rate and the mean excitation rate are shown in **b**. **b** | Application of the tonic inhibitory conductance reduced the slope of the I–O relationship (divisive operation, shown in green) and introduced an additive offset (subtractive operation, shown in orange). **c** | The relationship between the variance of random trains of synaptic conductances with constant amplitude and the total excitation rate (shown by grey circles). The variance increases with rate as predicted by Campbell's theorem. σ^2 is the conductance variance, ν is the total synaptic rate, and G(t) is the time course of the synaptic conductance waveform. **d** | The relationship between firing rate and mean voltage for control and during 1 nS tonic inhibition. In the presence of noise, this relationship is approximated by a power law, which when combined with conductance changes can perform a crude form of multiplication[81] (shown by solid green and grey lines). In contrast to the noise-free case (FIG. 3), a shunting inhibitory conductance has a multiplicative effect on the rate-coded input–output relationship owing to synaptic inputs exhibiting an excitation-dependent variance. Parts **a**, **b** and **d** are reproduced, with permission, from REF. 23 © (2003) Elesvier.

Input nonlinearities and gain modulation. Several studies of neurons in the primary visual cortex (V1) have focused on the roles of noise and the resulting power law of multiplicative operations on rate-coded signals[42,81,82], as this can potentially explain how neurons maintain their selectivity for stimulus orientation despite large changes in image contrast (contrast invariance)[42]. In an interesting twist to our understanding of the underlying computational mechanisms, the sensory input parameters in such models, which are often represented as sigmoidal and Gaussian functions, were shown to be crucial for gain modulation in the presence of a constant level of noise[93]. When such an additional nonlinear input is combined with a power law f_{out}–V_m relationship (fixed levels of noise), a robust output gain modulation occurs by simply altering conductance or adding current[93]. More recent work suggests that contrast invariance in V1 may arise from multiple mechanisms[94–96] and that neuronal gain modulation is associated with a simultaneous change in voltage noise and input resistance *in vivo*[97]. A related multiplicative transformation that is mediated by nonlinear Na^+ channels[98] has also been reported in the locust visual system, in neurons that are sensitive to looming objects. In summary, studies of the visual system highlight the importance of considering all of the linear and nonlinear components arising from the stimulus representation and synaptic input, together with noise and conductance, to understand how neuronal gain control is achieved in the brain.

Synaptic depression and gain modulation

The strength of synaptic connections that mediate driving input is often highly dynamic on short timescales (<10 s) and can increase (resulting in facilitation) or decrease (resulting in depression) with increasing frequency[99]. Frequency-dependent short-term depression (STD)[100,101] typically occurs when vesicle supply cannot keep up with the presynaptic firing rate[102–104] or when postsynaptic receptors desensitize[104,105]. Synapses exhibiting STD act as a low-pass filter to steady-state rate-coded inputs and preferentially transmit dynamic changes in rate, allowing neurons to respond to changes in signals rather than their absolute rate[106–108]. Theoretical studies show that STD introduces saturation of the neuronal I–O relationship and can enable synapse-specific neuronal gain control[96,107,109].

Recently, STD has also been shown to affect the arithmetic operations produced by changes in shunting inhibition in morphologically simple CGCs[110] (FIG. 6a). How does the presence of STD in the excitatory input affect the neuronal computation performed by a modulatory inhibitory input? The first clue came from the observation that CGCs integrate excitatory conductance from depressing and non-depressing synaptic conductances in a similar way (FIG. 6b). The second clue came from the relationship between presynaptic input rate and the time-averaged excitatory synaptic conductance, which was a saturating exponential function (FIG. 6c). This frequency-dependent nonlinearity introduced by STD transforms inhibition-induced additive shifts into a multiplicative gain change[110], thereby increasing the gain change performed by tonic inhibition by fourfold compared with that induced by noise alone (FIG. 6d). The size of the gain modulation depends on both the level of inhibition and the level of STD, and there is always a residual additive component (FIG. 6d). The time course of STD-based gain modulation depends on the input frequency and how quickly the synapse depresses to a steady-state level. Cerebellar mossy fibres fire up to 1 kHz *in vivo*[111], resulting in the rapid onset of STD[104] and fast STD-based gain modulation (4–75 ms) at the synapses between mossy fibres and granule cells[110]. However, STD-based gain modulation at synapses that are tuned for low firing rates will be slower.

To determine whether STD-based gain control operates on distributed synaptic input in morphologically complex neurons, synaptic integration was simulated in a multi-compartment layer 5 (L5) pyramidal neuron model[110] (FIG. 6e). When the amplitude of each of the 400 excitatory synaptic conductances was fixed, altering the rate of 30 inhibitory inputs (both excitatory and inhibitory inputs were randomly distributed over the basolateral dendritic tree) produced a largely additive shift in the sustained rate-coded I–O relationship (FIG. 6f). This is consistent with the prevailing view that distributed, asynchronous inputs are integrated in a linear manner[112–116]. By contrast, when STD was included in the excitatory inputs, excitatory and inhibitory synaptic inputs were multiplied together, producing robust gain changes (FIG. 6g). Different levels of inhibition scaled down the dynamic range of the I–O relationship in pyramidal cell simulations and in experiments with CGCs, showing that inhibition results in gain modulation of the output (FIG. 1f) rather than the input (FIG. 1e). As STD converts additive operations into multiplicative operations, it should enable rate-coded synaptic inputs that are located anywhere on the soma or dendrites to be multiplied together. Indeed, the fact that STD is more pronounced for distal synapses on L5 neurons[117,118] raises the possibility that this mechanism combines spatially separate inputs in these cells in a multiplicative manner[110]. Moreover, as STD can increase with long-term potentiation[119] or decrease with long-term depression[120], these arithmetic operations may depend on prior activity of the connection and thus potentially encode learning and routing of information through networks[46].

Low-pass filter
A device that attenuates high frequency signals but allows low frequency signals to pass unhindered.

The role of dendrites in neuronal arithmetic

As the field of dendritic computation has been discussed extensively in several excellent recent reviews[121–125] and in a book[126], in the remaining sections we will only highlight specific examples of how dendritic mechanisms may carry out arithmetic operations and the coding regimes under which they are likely to operate.

Linear dendritic integration. As discussed earlier, when synaptic inputs are distributed over the dendritic tree they tend to sum approximately linearly owing to the passive properties of dendrites[114–116,127]. But when inputs are clustered one would expect sublinear EPSP summation owing to a greater reduction in driving force and membrane shunting. However, nonlinear dendritic conductances — such as NMDA (*N*-methyl-D-aspartate) receptors, Na^+ channels and Ca^{2+} channels — can boost synaptic potentials when depolarized, whereas A-type K^+ conductances can dampen them[112,128,129]. A balance of these active conductances has been shown to underlie linear summation of synaptic inputs on the same dendritic branch of cultured pyramidal cells, counteracting nonlinearities introduced by reduced driving force and shunting[112,113]. Spines have also been proposed to promote linear synaptic integration by introducing a resistance that protects the main dendrite from the shunting effects of the synaptic conductance[130,131]. However, this mechanism requires that spine necks have a high resistance, a feature that is not supported by recent voltage dye measurements in the same cells, which provided estimates of ≤500 mΩ and an attenuation of somatic EPSPs of <15%[132]. Changes in shunting inhibition alone tend to produce subtractive effects on asynchronous rate-coded signals in complex cells due to the remote input and low noise (FIG. 6f), but a recent theoretical study suggests that by controlling the level of attenuation of current flowing from the dendrite to the soma, shunting inhibition could reduce neuronal gain[133]. However, it is unclear whether this would work effectively for discrete synaptic conductances and it is also unclear how dependent the gain modulation is on the dendritic location of the inhibitory shunt, as this can have a big effect on EPSP scaling[2,4,5,8,27,57,58].

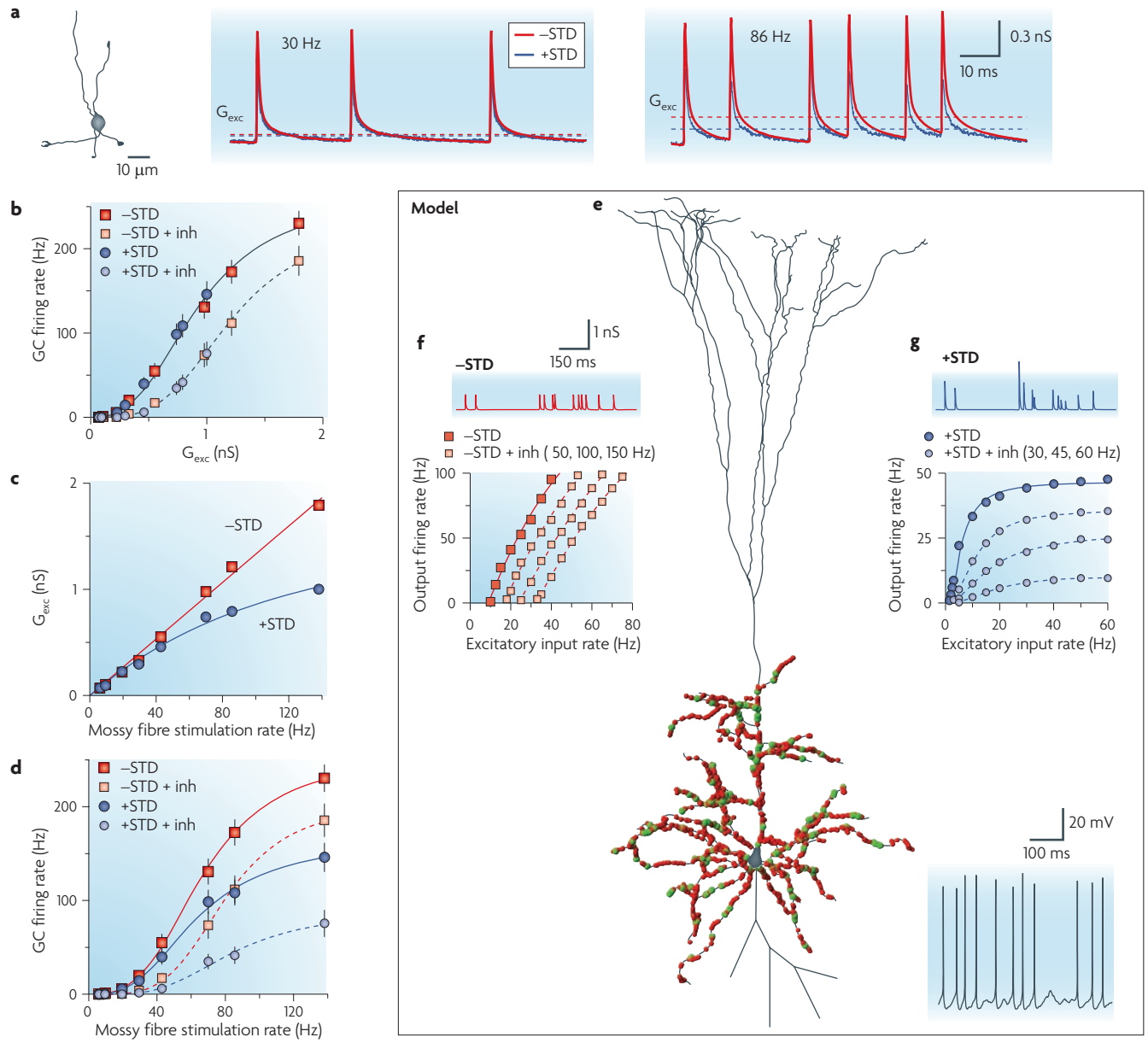

Figure 6 | **Short-term synaptic depression converts inhibition-mediated additive shifts in the rate-coded input–output relationship into multiplicative gain changes in morphologically simple and complex cells. a** | A morphologically simple cerebellar granule cell (CGC) with AMPAR (α-amino-3-hydroxy-5-methyl-4-isoxazole propionic acid receptor)-mediated synaptic conductance trains showing short-term depression (+STD; shown by blue traces) measured by stimulating mossy fibres at two frequencies. Artificial synaptic conductance trains without STD were also constructed (–STD; shown by red traces). Dashed lines show the time averaged conductance (G_{exc}) with and without STD. **b** | The relationship between CGC firing rate and G_{exc} obtained with the dynamic clamp technique. Depressing and non-depressing synaptic conductance trains produced similar CGC firing rates in control conditions and during a 0.5 nanosiemens (nS) constant (tonic) inhibitory conductance, indicating that they are integrated in a similar manner. Lines are fits to Hill-type functions (Supplementary information S1 (box)) and error bars show the standard error of the mean. **c** | The relationship between G_{exc} and mean input rate across four inputs with and without STD. Without STD the relationship is linear, as expected for summing identical waveforms. STD introduces a nonlinear saturating exponential function between input rate and G_{exc}. **d** | CGC input–output (I–O) relationships with and without STD and their modulation by a 0.5 nS tonic inhibitory conductance. STD in the driving input (**c**) amplifies the gain change observed with tonic inhibition by transforming the additive component into a multiplicative scaling. **e** | A morphologically complex layer 5 pyramidal neuron model[178]. The model shows random locations of excitatory synapses (shown by red circles) and inhibitory synapses (shown by green circles) distributed over the basolateral dendritic tree[110], and spiking is shown below. This simulation was built with neuroConstruct[172] and run on the NEURON simulator[179]. **f** | A conductance train and the I–O relationship for non-depressing excitatory synaptic input (–STD) for control conditions (shown by red squares) and for various rates of synaptic inhibition (shown by yellow squares). Synaptic inhibition introduced an additive shift along the driving axis consistent with linear integration. **g** | Same as **f** but including STD in the excitatory synaptic inputs (+STD alone, shown by dark blue circles; +STD and inhibition, shown by grey circles). STD changed the effects of inhibition from largely additive (**f**) to a largely multiplicative operation (**g**). Scaling down of the I–O relationship indicates an output gain modulation (FIG. 1f). Synaptic conductance waveforms and STD used in the simulation were matched to experimental data for layer 5 synaptic connections[110]. Part **a** is modified, with permission, from REF. 90 © (2003) Society for Neuroscience. Parts **b**–**g** are modified, with permission, from Nature REF. 110 © (2009) Macmillan Publishers Ltd. All rights reserved.

Nonlinear dendritic integration of spatially segregated inputs. Synaptic inputs from different neuronal sources can be located on spatially distinct subregions of the dendritic tree. Cortical L5 pyramidal cells are a particularly striking example, with distinct synaptic inputs on the basolateral dendrites in L5 and apical tufts in layer 1 at a distance of approximately 1 mm from the soma. Detecting temporally correlated synaptic input across layers raises a number of difficulties for the cell. Firstly, synaptic integration varies with location; a shorter time-window is required for combining synaptic inputs at distal locations (~10 ms) than at the soma (~50 ms window), because the dendritic EPSP has faster kinetics due to the shorter membrane time constant in the dendrite[117]. Secondly, modest synaptic inputs to the apical tufts produce only weak responses at the soma[117] because they are heavily attenuated as they propagate along the dendrite, as predicted by cable theory[7,134]. However, synaptic inputs can be amplified by Na^+ conductances in basal dendrites[129,135] and the apical tufts[127,136,137] of pyramidal cells. Active dendritic conductances may therefore alter the impact of synapses at different locations on the dendritic tree[138,139]. Moreover, Ca^{2+} conductances in the apical dendrite of L5 cells can amplify coincident synaptic input at the tuft and generate dendritic spikes[136,140–142]. Back-propagating APs lower the threshold for these Ca^{2+} dendritic spikes, thereby enabling the cell to associate spatially separated signals[141]. The impact of spatially segregated, temporally correlated synaptic inputs therefore depends on both the type of voltage-dependent conductances and their spatial distribution in the dendritic membrane.

Pyramidal cells also provide clear examples of how active dendritic conductances can contribute to gain modulation of segregated inputs during sustained firing. Dendritic recordings show that sustained injection of current noise into the distal dentritic tuft can increase the gain and reduce the rheobase of the firing rate–current response at the soma[143]. This multiplication of spatially separated inputs is predominantly due to Ca^{2+} channels[143], but persistent Na^+ channels may contribute to some boosting effects[137,144] and cancel subtractive effects by shifting the I–O relationship to the left[135]. A robust divisive gain modulation of the firing rate–current relationship was observed in pyramidal cells of electric fish in the presence of a dendritic $GABA_A$ receptor conductance[145]. Dendritic Na^+ channels underlie this effect by supporting back-propagating APs, which produced brief depolarizing after-potentials (DAPs), counteracting the spike in AHP at the soma. Dendritic inhibition reduces the DAP by speeding up repolarization of the back-propagating APs, revealing a larger AHP at the soma and thus reduced neuronal gain[145,146]. By contrast, when inhibition was applied to the soma, the back-propagating AP, DAP and AHP were unaffected and inhibition produced a conventional subtractive shift in the I–O relationship. This potentially enables inhibitory interneuron populations that specifically target dendrites or the soma to carry out distinct arithmetic operations on sustained rate-coded inputs[145]. These nonlinear dendritic mechanisms may enable pyramidal cells to combine spatially segregated synaptic inputs in a multiplicative manner, both for sparse temporally correlated and sustained rate-coded signalling regimes.

Nonlinear dendritic integration of spatially clustered synapses. Clustered excitatory synaptic inputs may produce a sufficiently large local depolarization to activate nonlinear dendritic mechanisms. Theoretical work suggests that such reductions in driving force in the dendrite could saturate the synaptic response and amplify inhibition- and noise-mediated gain modulation of sustained rate-coded signals[79]. Local depolarizations may also trigger regenerative dendritic events mediated by voltage-gated conductances. Dendritic Na^+ channels have been shown to amplify subthreshold EPSPs in a multiplicative manner and speed their rise[116,129,135,137]. Regenerative dendritic Na^+ spikes in pyramidal cells[129,147,148] can be localized to specific branches, modified in a branch-specific manner[149] and selectively activated by synaptic inputs that are clustered in space and time[116,127,150–152]. These features have generated considerable interest because they may enable individual dendritic branches to act as nonlinear thresholding units. Experiments using two-photon glutamate uncaging to mimic different patterns of synaptic input suggest that ~20 synaptic inputs (~5% of the total) are required to trigger a local dendritic Na^+ spike in radial oblique dendrites of CA1 pyramidal cells[151]. Dendritic patching of basal dendrites of L5 pyramidal cells gave comparable estimates and revealed rapidly decaying EPSPs, with a space constant of only 50 μm, indicating that voltage changes can be localized to an individual branch[127]. The rapid membrane time constant in these fine dendrites means that local synaptic inputs have to be highly synchronized (3–6 ms time-window) to trigger a dendritic Na^+ spike[117,127,151]. These properties, together with the fact that dendritic Na^+ spikes are suppressed for hundreds of milliseconds following a spike owing to Na^+ channel inactivation (whether triggered locally within a branch[152] or globally across the dendrite by a back-propagating AP[129,152]), suggest that these dendritic Na^+ conductances are tuned to amplify sparse, temporally correlated inputs (FIG. 2), rather than to contribute to sustained rate-coded signalling[112–116]. By selectively increasing the gain of dendritic branches that receive temporally correlated inputs, Na^+ conductances may form distinct computational compartments and enhance the precision of spike output[153]. Such dendritic-branch-specific thresholding units may substantially enhance the computational power of a neuron[154,155] and may potentially link together to form a functional structure that is analogous to a two-layer neural network (FIG. 7d) with comparable computational power[156,159].

Synaptic NMDA receptors (NMDARs) can also amplify clustered synaptic inputs (FIG. 7a,b). Their highly nonlinear voltage-dependence, which is caused by the Mg^{2+} block of the NMDAR channel[158], can produce

Cable theory
This refers to the mathematical equations that describe how electrical signals propagate in space and time in spatially extended neurons.

Two-photon glutamate uncaging
The release of glutamate from a 'caged' glutamate compound using two-photon excitation.

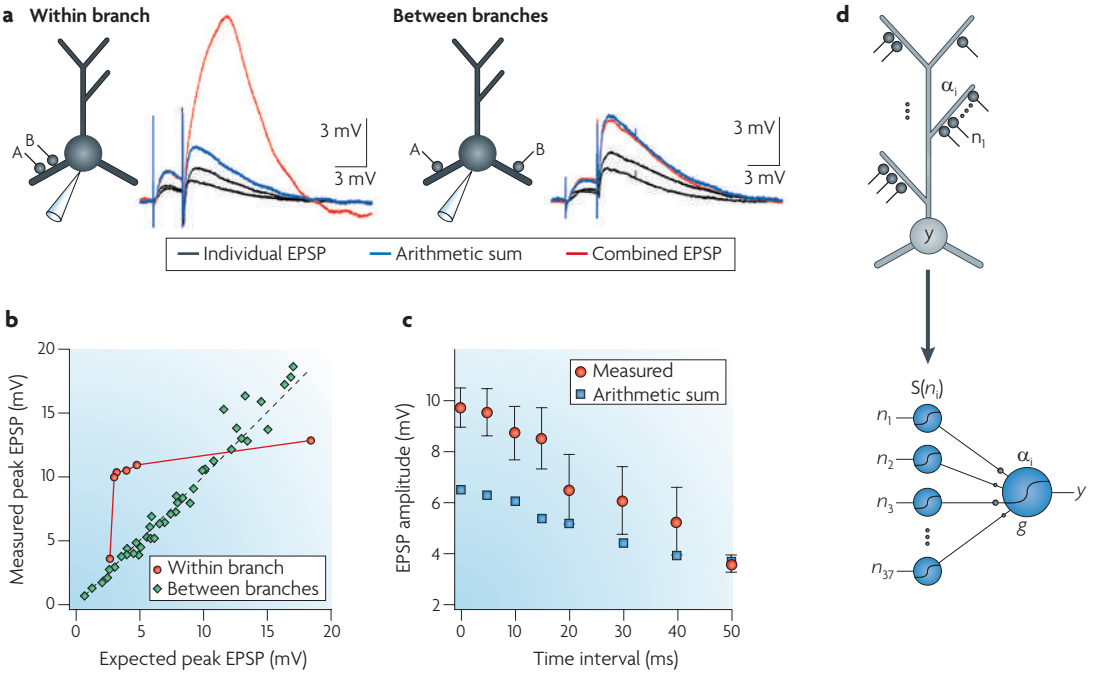

Figure 7 | **Clustered synaptic input activates local dendritic nonlinearities which could form the basis of branch specific computation. a** | Cartoons showing layer 5 cortical pyramidal cells with the location of activated synaptic inputs and the recording electrode. 'Within branch' refers to two inputs (A and B) that synapse onto the same dendritic branch (left), and 'between branches' corresponds to two inputs that synapse onto different branches (right). Traces show the somatic responses to a paired-pulse synaptic stimulation protocol. Black traces show the two synaptic inputs stimulated individually, blue traces show the predicted response for simultaneous activation (assuming linear summation) and red traces show the measured response for intermediate strength stimulation. The within-branch response was supralinear, whereas the response between branches was linear. This effect was blocked by a selective NMDAR (*N*-methyl-D-aspartate receptor) antagonist. **b** | Responses for the two input scenarios; the between-branches configuration (shown in green; the dashed line indicates linearity) and the within-branch configuration (shown in red). The nonlinear effects of NMDARs are seen when excitatory postsynaptic potentials (EPSPs) are a few millivolts in amplitude. However, these experiments were carried out in the presence of a $GABA_A$ (α-aminobutyric acid type A) receptor antagonist, which may favour the occurrence of NMDA spikes[161]. **c** | The difference between the arithmetic sum of individual inputs (shown by blue squares) and paired-pulse protocols with different intervals between the pulses. The supralinear response of the within-branch configuration occurs when the two synaptic inputs occur within approximately 40 ms indicates that synaptic NMDAR activation has a 'memory' of prior input onto the branch over this timescale. **d** | A cartoon of a pyramidal cell with n_i clustered synaptic inputs on each of the dendritic branches. A nonlinear dendritic mechanism, such as NMDAR spikes, introduces a nonlinear sigmoidal input–output function (S(n_i)) to each of the subcompartments. The weights of the subcompartments (α_i) are then combined with the somatic spike threshold nonlinearity (*g*) to produce output (*y*). It has been proposed that the presence of multiple dendritic subcompartments each with a nonlinear thresholding element could enable an individual pyramidal cell to act like a two-layer network of neurons, thereby enhancing its computational power. Parts **a**–**c** modified, with permission, from *Nature Neuroscience* REF. 156 © (2004) Macmillan Publishers Ltd. All rights reserved. Part **d** modified, with permission, from REF. 157 © (2003) Elsevier.

regenerative voltage depolarizations in the dendrite[159]. These so-called NMDAR spikes are spatially restricted to sites of synaptic input owing to their glutamate-dependence and are unlikely to actively propagate[159]. NMDAR spikes last 50–100 ms[156,159,160], but modelling predicts that they can be curtailed by smaller inhibitory synaptic conductances on the dendrite[161]. NMDARs on hyperpolarized regions of the dendrite exhibit a 'memory' of the prior synaptic activity for the 40 ms or so that glutamate (and glycine) remains bound to the receptors[156]. This can be 'unlocked' upon depolarization, when the Mg^{2+} block of the channel is relieved, allowing glutamate-bound NMDARs to pass current. This mechanism, which can amplify subsequent glutamatergic inputs to the same dendrite[156] (FIG. 7c), is local because the space constant for the EPSP is short in thin dendrites of pyramidal cells[127]. A number of other differences between Na^+ spikes and NMDAR spikes are worth noting. NMDAR spikes are slower rising and the time-window for coincidence of the presynaptic inputs is tenfold larger than for Na^+ spikes, allowing activation with less temporal precision. In addition, the duration of the NMDAR spike is sufficiently long to act as a coincident detector and also interact with short-duration rate-coded bursts of input. Lastly, NMDARs do not become inactivated as rapidly as dendritic Na^+ channels,

a feature that might be important during sustained firing. NMDARs are an attractive local nonlinear dendritic mechanism that could alter neuronal gain depending on the spatio-temporal correlation of the input. However, it is presently unclear how robust NMDAR spikes are in the presence of the substantial inhibitory input that occurs *in vivo*[54,161].

Although nonlinear dendritic mechanisms have been discussed separately, in reality a dendritic excitability is determined by a combination of dendritic conductances. Indeed, a recent study suggests that clustered synaptic inputs onto multiple thin dendrites in the tuft of L5 pyramidal cells can be amplified by both NMDAR and Na^+ channels and then trigger a forward-propagating Ca^{2+} spike in the apical dendrite[136]. Nonlinear dendritic mechanisms that are activated by clustered inputs require that synapses project to a particular dendritic branch and that their spike latencies are restricted to just a few milliseconds. Such mechanisms are likely to increase the gain of the P_{spike}–σ_{input} relationship, potentially allowing better discrimination of spatio-temporal patterns of synaptic input in sparse coding regimes[162]. However, the precise spatio-temporal correlations required for activation of local dendritic nonlinearities impose exacting constraints, given the temporal variability of sensory input and the fact that many excitatory axons project diffusely onto multiple dendritic branches. Indeed, a recent two-photon imaging study of dendritic visual processing *in vivo* found no evidence for segregation of orientation tuning onto specific branches[163]. Nevertheless, a recent study that modelled synaptic activation in L5 cells predicted that NMDAR spikes could also be activated by inputs distributed randomly over the apical tuft region[136]. Determining the importance of clustered synaptic inputs for dendritic computation will require a better understanding of the functional connectivity of networks in the brain.

Conclusions

Arithmetic operations allow neurons to combine and transform different signals and to discriminate spatial and temporal correlations in their synaptic inputs. This Review shows that both morphologically simple and complex neurons possess a number of biophysical mechanisms that enable them to perform rapid arithmetic operations on signals encoded in different ways (FIG. 8). However, the presence of multiple interacting nonlinear mechanisms and stochastic noise, together with the often mixed additive and multiplicative components of arithmetic operations has made the unequivocal identification of the underlying biophysical mechanisms difficult. Nevertheless, a number of conclusions can be drawn from studies in this rapidly expanding field.

Relationship between biophysical mechanisms and coding regimes. Although information is likely to be encoded by APs on a continuum of timescales[47], at the limits neurons can act either as integrators of sustained rate-coded inputs or as coincidence detectors of sparse temporally correlated signals. Appreciation of this apparent dichotomy of coding can help to define the neuronal I–O relationship and identify the arithmetic operation being performed, as well as the underlying biophysical mechanisms (FIG. 8). Synaptic noise, which fundamentally changes the integration properties of neurons, can have similar multiplicative and additive effects on I–O relationships under sparse temporal and sustained rate-coded regimes. Changes in synaptic noise can therefore be considered a general mechanism for neuronal arithmetic.

Other mechanisms seem tuned for particular coding regimes. For example, changes in shunting inhibition, in concert with high levels of synaptic-input-dependent noise[23,77], synaptic STD[110], dendritic Na^+ channels (which can produce a DAP)[145] or an input-dependent nonlinearity[93], can only control neural gain under sustained rate-coded signalling regimes, as conductance changes produce additive shifts during temporally correlated signalling[73]. In sparse signalling regimes, nonlinear dendritic conductances — such as Na^+ channels in CA1 cells — seem to be best suited to act as coincidence detectors[151], as they amplify the EPSP during spatio-temporally correlated inputs and inactivate[152] under sustained firing conditions. There are also mechanisms that fall between these coding extremes and that are not as general as noise and conductance; NMDA receptors are well suited to act as spatio-temporal coincidence detectors with a longer integration window than for Na^+ channels and may also be able to interact with brief rate-coded bursts[136,156]. In summary, different nonlinear processes seem to operate under sustained rate-coding and sparse temporally correlated signalling regimes, allowing neurons to perform arithmetic computations on information that is encoded in different ways.

Simple and complex cells — local and segregated mechanisms. Even the simplest of neurons, such as CGCs, can perform neuronal arithmetic (FIG. 8). Experiments on these cells show that computations depend on the properties of the synaptic input: shunting inhibition performs a subtractive operation on the I–O relationship when excitation is mediated by noise-free conductance steps, but in the presence of input-dependent noise and STD, these neurons perform a largely multiplicative operation[23,110]. Both simple and complex cells can use these synaptic mechanisms to transform the linear integration of excitatory and inhibitory conductances into nonlinear multiplicative operations (FIG. 8). In contrast to simple cells, the dendritic trees of morphologically complex cells often form multiple interconnected electrical compartments. Dendritic nonlinearities can be used to counteract local nonlinear driving force in these compartments — which allows linear additive integration[112,113] — or they can be used to multiply together synaptic inputs on different parts of the dendrite. Shunting inhibition combined with noise changes[66] and/or STD[110], can perform these functions during sustained rate-coded signalling, as can dendritic Ca^{2+} conductances[143] and dendritic inhibition combined with dendritic Na^+ channels that support back-propagating APs and DAPs[145]. Complex

cells can also perform local processing; dendritic Na^+ channels (in CA1 cells[151]) and NMDAR spikes[156] only become activated with clustered synaptic input and may enable dendritic-branch-specific computations of temporally coded signals.

Neurons are endowed with an extensive 'tool kit' of biophysical mechanisms that enable them to perform arithmetic operations on their synaptic inputs, irrespective of whether they are morphologically simple or complex or whether they operate as integrators of sustained rate-coded input or coincident detectors of sparse temporally correlated signals (FIG. 8). The existence of such a tool kit suggests that the individual neurons are powerful computational devices in their own right.

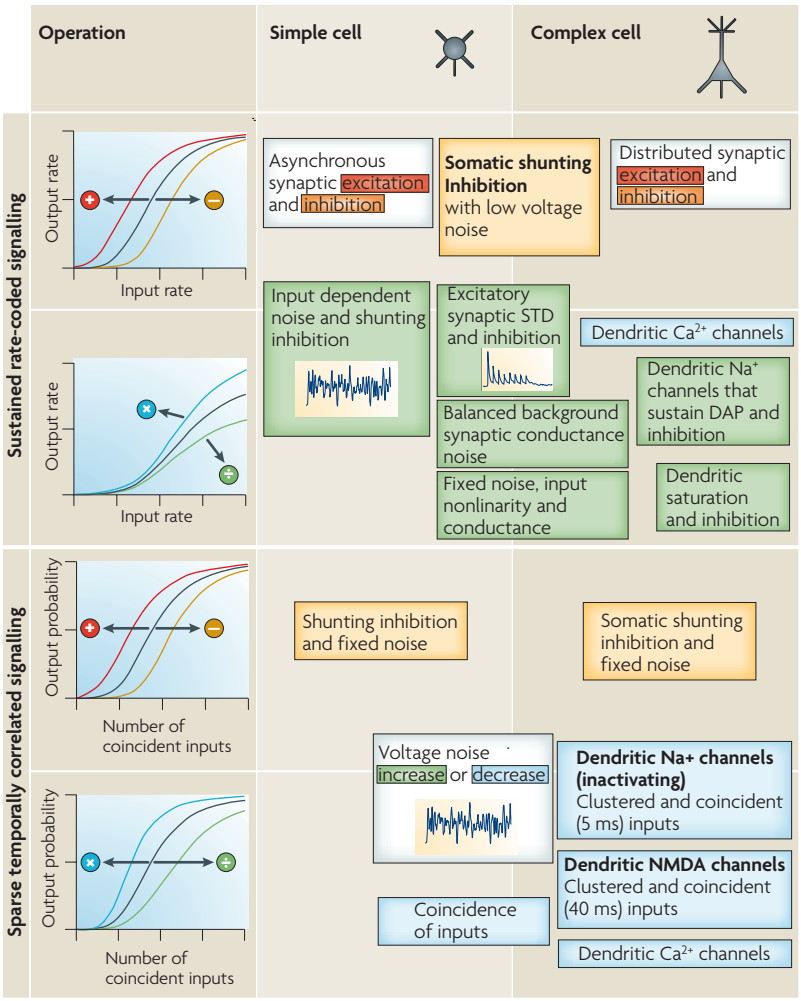

Figure 8 | **Summary of biophysical mechanisms underlying rapid neuronal arithmetic.** Mechanisms that may underlie rapid addition (shown in red) and subtraction (shown in orange) or multiplication (shown in blue) and division (shown in green) of synaptic input in cells with simple and complex morphologies. The upper two rows correspond to sustained rate-coded signalling while the bottom two correspond to sparse temporally coded signalling. As indicated by the graphs on the left, rows one and three correspond to additive operations, whereas rows two and four correspond to multiplicative operations. Overlap of boxes between additive and multiplicative regions indicates mixed operations. DAP, depolarizing after potential; NMDA, *N*-methyl-D-aspartate; STD, short term depression.

Future directions

What types of neural computation occur* in vivo*? A key challenge in neuronal computation is to establish which of the potential biophysical mechanisms identified are actually used for specific computational tasks in the brain. Most work on neural computation to date has relied on electrophysiology and uncaging methods in acute slice preparations or on modelling. Although some *in vivo* studies support the existence of specific mechanisms, such as STD-[164], noise-, and conductance-based gain modulation[43,97] and dendritic processing[163,165,166], further *in vivo* investigations are required to confirm which mechanisms are involved in neuronal arithmetic. It will also be important to test the hypothesis that dendritic trees of complex neurons act as multi-compartment processors[155] by establishing whether spatial clustering of synaptic connectivity occurs[163,167] and whether the temporal coincidence of sensory-evoked inputs are sufficiently precise to activate local dendritic nonlinearities. Although these questions are difficult to address *in vivo* without anaesthetics, which can change neuronal excitability and synaptic conductances[168], recent technological advances that allow whole-cell patch-clamp recordings[169] and two-photon imaging to be carried out in awake animals[170] suggest that this type of study is now feasible.

Linking* in vivo *to* in vitro *and modelling. Information from *in vivo* recordings can make *in vitro* experiments and computer models more realistic and predictions more reliable. Acute slice preparations allow manipulation and control of neuronal activity, rendering this preparation invaluable for investigating neural computation. However, new approaches are required to reproduce *in vitro* the spatial and temporal patterns of activation onto dendritic trees observed *in vivo*[163,165] and to examine the fine connectivity patterns in neural networks[171]. Such information is relatively easy to implement in models with interoperable software tools, such as neuroConstruct, which allows the creation of three-dimensional network models with a high degree of anatomical and physiological detail[172] (FIG. 6), but these patterns are more difficult to reproduce *in vitro*. Realistic synaptic-like conductances can be mimicked with a dynamic clamp[23,51,66,73,74,110,173], but this technique has limitations for complex neurons because conductance injection is usually restricted to the soma. Two-photon glutamate uncaging is currently the most precise way to mimic different spatio-temporal input patterns, but available caged glutamate compounds block inhibitory transmission[174] and are relatively insensitive to two-photon excitation, necessitating high light-powers, which can be phototoxic[175]. New caged compounds[176] and optogenetic methods[177] provide powerful alternative approaches, potentially allowing *in vivo* patterns of activity to be reproduced *in vitro*. With these newly emerging experimental and modelling technologies, it will be possible to gain a deeper understanding of the mechanistic basis of neural arithmetic and to identify which mechanisms are used by the brain to solve the complex computational problems that we experience every day.

1. McCulloch, W. S. & Pitts, W. A logical calculus of the ideas immanent in nervous activity. *Bull. Math. Biophys.* **5**, 115–133 (1943).
2. Blomfield, S. Arithmetical operations performed by nerve cells. *Brain Res.* **69**, 115–124 (1974).
A pioneering theoretical study that predicted that synaptic interactions in a single neuron could be additive or multiplicative.
3. Barlow, H. B. & Levick, W. R. The mechanism of directionally selective units in rabbit's retina. *J. Physiol.* **178**, 477–504 (1965).
4. Koch, C., Poggio, T. & Torre, V. Nonlinear interactions in a dendritic tree: localization, timing and role in information processing. *Proc. Natl Acad. Sci. USA* **50**, 2799–2802 (1983).
5. Jack, J. J. B., Noble, D. & Tsien, R. W. *Electric Current Flow in Excitable Cells* (Clarendon Press, Oxford, 1975).
6. Rall, W. in *Neuronal Theory and Modeling* (ed. Reiss, R. F.) 73–97 (Stanford Univ. Press, 1964).
7. Rall, W., Burke, R. E., Smith, T. G., Nelson, P. G. & Frank, K. Dendritic location of synapses and possible mechanisms for the monosynaptic EPSP in motoneurons. *J. Neurophysiol.* **30**, 1169–1193 (1967).
8. Torre, V. & Poggio, T. A synaptic mechanism possibly underlying directional selectivity to motion. *Proc. R. Soc. Lond. B* **202**, 409–416 (1978).
9. Braitenberg, V. Brain size and number of neurons: an exercise in synthetic neuroanatomy. *J. Comput. Neurosci.* **10**, 71–77 (2001).
10. Adrian, E. D. & Zotterman, Y. The impulses produced by sensory nerve endings. Part 3. Impulses set up by touch and pressure. *J. Physiol.* **61**, 465–483 (1926).
11. Adrian, E. D. & Zotterman, Y. The impulses produced by sensory nerve-endings. Part 2. The response of a single end-organ. *J. Physiol.* **61**, 151–171 (1926).
12. Arenz, A., Silver, R. A., Schaefer, A. T. & Margrie, T. W. The contribution of single synapses to sensory representation *in vivo*. *Science* **321**, 977–980 (2008).
13. Vinje, W. E. & Gallant, J. L. Sparse coding and decorrelation in primary visual cortex during natural vision. *Science* **287**, 1273–1276 (2000).
14. Olshausen, B. A. & Field, D. J. Sparse coding of sensory inputs. *Curr. Opin. Neurobiol.* **14**, 481–487 (2004).
15. Kerr, J. N. *et al.* Spatial organization of neuronal population responses in layer 2/3 of rat barrel cortex. *J. Neurosci.* **27**, 13316–13328 (2007).
16. Brecht, M., Roth, A. & Sakmann, B. Dynamic receptive fields of reconstructed pyramidal cells in layers 3 and 2 of rat somatosensory barrel cortex. *J. Physiol.* **553**, 243–265 (2003).
17. Margrie, T. W., Brecht, M. & Sakmann, B. *In vivo*, low-resistance, whole-cell recordings from neurons in the anaesthetized and awake mammalian brain. *Pflugers Arch.* **444**, 491–498 (2002).
18. Brecht, M. & Sakmann, B. Dynamic representation of whisker deflection by synaptic potentials in spiny stellate and pyramidal cells in the barrels and septa of layer 4 rat somatosensory cortex. *J. Physiol.* **543**, 49–70 (2002).
19. Földiák, P. in *The Handbook of Brain Theory and Neural Networks.* (ed. Arbib, M. A.) 1064–1068 (MIT Press, 2002).
20. Levy, W. B. & Baxter, R. A. Energy efficient neural codes. *Neural Comput.* **8**, 531–543 (1996).
21. Attwell, D. & Laughlin, S. B. An energy budget for signaling in the grey matter of the brain. *J. Cereb. Blood Flow Metab.* **21**, 1133–1145 (2001).
22. Holt, G. R. & Koch, C. Shunting inhibition does not have a divisive effect on firing rates. *Neural Comput.* **9**, 1001–1013 (1997).
An influential theoretical study that predicted that shunting inhibition has a subractive effect on the rate-coded I–O relationship. It includes an elegant analysis of why inhibitory shunting conductances behave like current sources during sustained firing.
23. Mitchell, S. J. & Silver, R. A. Shunting inhibition modulates neuronal gain during synaptic excitation. *Neuron* **38**, 433–445 (2003).
Experimental study on CGCs that shows that neuronal gain can be modulated by a shunting inhibitory conductance when excitation is mediated by noisy rate-coded synaptic inputs.
24. McCormick, D. A. Neurotransmitter actions in the thalamus and cerebral cortex and their role in neuromodulation of thalamocortical activity. *Prog. Neurobiol.* **39**, 337–388 (1992).
25. Salinas, E. & Thier, P. Gain modulation: a major computational principle of the central nervous system. *Neuron* **27**, 15–21 (2000).
26. Salinas, E. & Sejnowski, T. J. Gain modulation in the central nervous system: where behavior, neurophysiology, and computation meet. *Neuroscientist* **7**, 430–440 (2001).
27. Skydsgaard, M. & Hounsgaard, J. Spatial integration of local transmitter responses in motoneurones of the turtle spinal cord *in vitro*. *J. Physiol.* **479**, 233–246 (1994).
28. Granit, R., Kernell, D. & Lamarre, Y. Algebraical summation in synaptic activation of motoneurones firing within the 'primary range' to injected currents. *J. Physiol.* **187**, 379–399 (1966).
29. Ma, W. J., Beck, J. M., Latham, P. E. & Pouget, A. Bayesian inference with probabilistic population codes. *Nature Neurosci.* **9**, 1432–1438 (2006).
30. Yang, T. & Shadlen, M. N. Probabilistic reasoning by neurons. *Nature* **447**, 1075–1080 (2007).
31. Brenner, N., Bialek, W. & de Ruyter van Steveninck, R. Adaptive rescaling maximizes information transmission. *Neuron* **26**, 695–702 (2000).
32. Andersen, R. A., Essick, G. K. & Siegel, R. M. Encoding of spatial location by posterior parietal neurons. *Science* **230**, 456–458 (1985).
33. Andersen, R. A. & Mountcastle, V. B. The influence of the angle of gaze upon the excitability of the light-sensitive neurons of the posterior parietal cortex. *J. Neurosci.* **3**, 532–548 (1983).
34. Brotchie, P. R., Andersen, R. A., Snyder, L. H. & Goodman, S. J. Head position signals used by parietal neurons to encode locations of visual stimuli. *Nature* **375**, 232–235 (1995).
35. Salinas, E. & Abbott, L. F. Transfer of coded information from sensory to motor networks. *J. Neurosci.* **15**, 6461–6474 (1995).
36. Pouget, A. & Sejnowski, T. J. Spatial transformations in the parietal cortex using basis functions. *J. Cogn. Neurosci.* **9**, 222–237 (1997).
37. Zipser, D. & Andersen, R. A. A back-propagation programmed network that simulates response properties of a subset of posterior parietal neurons. *Nature* **331**, 679–684 (1988).
38. Yakusheva, T. A. *et al.* Purkinje cells in posterior cerebellar vermis encode motion in an inertial reference frame. *Neuron* **54**, 973–985 (2007).
39. McAdams, C. J. & Maunsell, J. H. Effects of attention on orientation-tuning functions of single neurons in macaque cortical area V4. *J. Neurosci.* **19**, 431–441 (1999).
40. Treue, S. & Martinez Trujillo, J. C. Feature-based attention influences motion processing gain in macaque visual cortex. *Nature* **399**, 575–579 (1999).
41. Tovee, M. J., Rolls, E. T. & Azzopardi, P. Translation invariance in the responses to faces of single neurons in the temporal visual cortical areas of the alert macaque. *J. Neurophysiol.* **72**, 1049–1060 (1994).
42. Anderson, J. S., Lampl, I., Gillespie, D. C. & Ferster, D. The contribution of noise to contrast invariance of orientation tuning in cat visual cortex. *Science* **290**, 1968–1972 (2000).
An experimental study that highlighted the importance of noise in contrast invariance of orientation tuning and showed that it smoothed the relationship between output firing rate and membrane potential.
43. Ingham, N. J. & McAlpine, D. GABAergic inhibition controls neural gain in inferior colliculus neurons sensitive to interaural time differences. *J. Neurosci.* **25**, 6187–6198 (2005).
44. Engel, A. K., Fries, P. & Singer, W. Dynamic predictions: oscillations and synchrony in top-down processing. *Nature Rev. Neurosci.* **2**, 704–716 (2001).
45. Buzsaki, G. & Draguhn, A. Neuronal oscillations in cortical networks. *Science* **304**, 1926–1929 (2004).
46. Haider, B. & McCormick, D. A. Rapid neocortical dynamics: cellular and network mechanisms. *Neuron* **62**, 171–189 (2009).
47. Rudolph, M. & Destexhe, A. Tuning neocortical pyramidal neurons between integrators and coincidence detectors. *J. Comput. Neurosci.* **14**, 239–251 (2003).
48. Azouz, R. Dynamic spatiotemporal synaptic integration in cortical neurons: neuronal gain, revisited. *J. Neurophysiol.* **94**, 2785–2796 (2005).
49. Diesmann, M., Gewaltig, M. O. & Aertsen, A. Stable propagation of synchronous spiking in cortical neural networks. *Nature* **402**, 529–533 (1999).
50. Marsalek, P., Koch, C. & Maunsell, J. On the relationship between synaptic input and spike output jitter in individual neurons. *Proc. Natl Acad. Sci. USA* **94**, 735–740 (1997).
51. Williams, S. R. Spatial compartmentalization and functional impact of conductance in pyramidal neurons. *Nature Neurosci.* **7**, 961–967 (2004).
52. Koch, C., Douglas, R. & Wehmeier, U. Visibility of synaptically induced conductance changes: theory and simulations of anatomically characterized cortical pyramidal cells. *J. Neurosci.* **10**, 1728–1744 (1990).
53. Freund, T. F. & Katona, I. Perisomatic inhibition. *Neuron* **56**, 33–42 (2007).
54. Borg-Graham, L. J., Monier, C. & Fregnac, Y. Visual input evokes transient and strong shunting inhibition in visual cortical neurons. *Nature* **393**, 369–373 (1998).
55. Fatt, P. & Katz, B. The effect of inhibitory nerve impulses on a crustacean muscle fibre. *J. Physiol.* **121**, 374–389 (1953).
56. Coombs, J. S., Eccles, J. C. & Fatt, P. The electrical properties of the motoneurone membrane. *J. Physiol.* **130**, 396–413 (1955).
57. Vu, E. T. & Krasne, F. B. Evidence for a computational distinction between proximal and distal neuronal inhibition. *Science* **255**, 1710–1712 (1992).
58. Liu, G. Local structural balance and functional interaction of excitatory and inhibitory synapses in hippocampal dendrites. *Nature Neurosci.* **7**, 373–379 (2004).
59. Carandini, M. & Heeger, D. J. Summation and division by neurons in primate visual cortex. *Science* **264**, 1333–1336 (1994).
60. Nelson, M. L. A mechnism for neuronal gain control by decending pathways. *Neural Comput.* **6**, 242–254 (1994).
61. Gabbiani, F., Midtgaard, J. & Knöpfel, T. Synaptic integration in a model of cerebellar granule cells. *J. Neurophysiol.* **72**, 999–1009 (1994).
62. Capaday, C. A re-examination of the possibility of controlling the firing rate gain of neurons by balancing excitatory and inhibitory conductances. *Exp. Brain Res.* **143**, 67–77 (2002).
63. Sah, P. & Faber, E. S. Channels underlying neuronal calcium-activated potassium currents. *Prog. Neurobiol.* **66**, 345–353 (2002).
64. Berman, N. J., Douglas, R. J. & Martin, K. A. GABA-mediated inhibition in the neural networks of visual cortex. *Prog. Brain Res.* **90**, 443–476 (1992).
65. Brickley, S. G., Cull-Candy, S. G. & Farrant, M. Development of a tonic form of synaptic inhibition in rat cerebellar granule cells resulting from persistent activation of $GABA_A$ receptors. *J. Physiol.* **497**, 753–759 (1996).
66. Chance, F., Abbott, L. & Reyes, A. Gain modulation from background synaptic input. *Neuron* **35**, 773–782 (2002).
An experimental study on pyramidal cells that showed that neuronal gain could be altered by changing the level of noise introduced by balanced excitatory and inhibitory background synaptic input.
67. Ulrich, D. Differential arithmetic of shunting inhibition for voltage and spike rate in neocortical pyramidal cells. *Eur. J. Neurosci.* **18**, 2159–2165 (2003).
68. Destexhe, A. & Pare, D. Impact of network activity on the integrative properties of neocortical pyramidal neurons *in vivo*. *J. Neurophysiol.* **81**, 1531–1547 (1999).
69. Destexhe, A., Rudolph, M. & Pare, D. The high-conductance state of neocortical neurons *in vivo*. *Nature Rev. Neurosci.* **4**, 739–751 (2003).
70. Ho, N. & Destexhe, A. Synaptic background activity enhances the responsiveness of neocortical pyramidal neurons. *J. Neurophysiol.* **84**, 1488–1496 (2000).
An early theoretical study that predicted that background synaptic input enhances the responsiveness of neocortical pyramidal neurons to coincident synaptic input.
71. Sargent, P. B., Saviane, C., Nielsen, T. A., DiGregorio, D. A. & Silver, R. A. Rapid vesicular release, quantal variability, and spillover contribute to the precision and reliability of transmission at a glomerular synapse. *J. Neurosci.* **25**, 8173–8187 (2005).
72. Stacey, W. C. & Durand, D. M. Synaptic noise improves detection of subthreshold signals in hippocampal CA1 neurons. *J. Neurophysiol.* **86**, 1104–1112 (2001).

73. Shu, Y., Hasenstaub, A., Badoual, M., Bal, T. & McCormick, D. A. Barrages of synaptic activity control the gain and sensitivity of cortical neurons. *J. Neurosci.* **23**, 10388–10401 (2003).
A dynamic clamp study that showed that background noise controls the gain of the relationship between spike probability and excitatory conductance for coincident inputs, while voltage and conductance changes induce additive shifts. These effects are linked to up and down states.
74. Wolfart, J., Debay, D., Le Masson, G., Destexhe, A. & Bal, T. Synaptic background activity controls spike transfer from thalamus to cortex. *Nature Neurosci.* **8**, 1760–1767 (2005).
75. Fellous, J. M., Rudolph, M., Destexhe, A. & Sejnowski, T. J. Synaptic background noise controls the input/output characteristics of single cells in an *in vitro* model of *in vivo* activity. *Neuroscience* **122**, 811–829 (2003).
76. Destexhe, A., Rudolph, M., Fellous, J. M. & Sejnowski, T. J. Fluctuating synaptic conductances recreate *in vivo*-like activity in neocortical neurons. *Neuroscience* **107**, 13–24 (2001).
77. Doiron, B., Longtin, A., Berman, N. & Maler, L. Subtractive and divisive inhibition: effect of voltage-dependent inhibitory conductances and noise. *Neural Comput.* **13**, 227–248 (2001).
78. Tiesinga, P. H., Jose, J. V. & Sejnowski, T. J. Comparison of current-driven and conductance-driven neocortical model neurons with Hodgkin–Huxley voltage-gated channels. *Phys. Rev. E Stat. Phys. Plasmas Fluids Relat. Interdiscip. Topics* **62**, 8413–8419 (2000).
An early theoretical study that predicted that increasing the noise of the input conductance will reduce the gain of neurons during sustained firing.
79. Prescott, S. A. & De Koninck, Y. Gain control of firing rate by shunting inhibition: roles of synaptic noise and dendritic saturation. *Proc. Natl Acad. Sci. USA* **100**, 2076–2081 (2003).
80. Higgs, M. H., Slee, S. J. & Spain, W. J. Diversity of gain modulation by noise in neocortical neurons: regulation by the slow afterhyperpolarization conductance. *J. Neurosci.* **26**, 8787–8799 (2006).
81. Hansel, D. & van Vreeswijk, C. How noise contributes to contrast invariance of orientation tuning in cat visual cortex. *J. Neurosci.* **22**, 5118–5128 (2002).
82. Miller, K. D. & Troyer, T. W. Neural noise can explain expansive, power-law nonlinearities in neural response functions. *J. Neurophysiol.* **87**, 653–659 (2002).
83. Okun, M. & Lampl, I. Instantaneous correlation of excitation and inhibition during ongoing and sensory-evoked activities. *Nature Neurosci.* **11**, 535–537 (2008).
84. Galarreta, M. & Hestrin, S. Frequency-dependent synaptic depression and the balance of excitation and inhibition in the neocortex. *Nature Neurosci.* **1**, 587–594 (1998).
85. Shadlen, M. N. & Newsome, W. T. Noise, neural codes and cortical organization. *Curr. Opin. Neurobiol.* **4**, 569–579 (1994).
86. Kerr, A. M. & Capogna, M. Unitary IPSPs enhance hilar mossy cell gain in the rat hippocampus. *J. Physiol.* **578**, 451–470 (2007).
87. Pavlov, I., Savtchenko, L. P., Kullmann, D. M., Semyanov, A. & Walker, M. C. Outwardly rectifying tonically active $GABA_A$ receptors in pyramidal cells modulate neuronal offset, not gain. *J. Neurosci.* **29**, 15341–15350 (2009).
88. Longtin, A., Doiron, B. & Bulsara, A. R. Noise-induced divisive gain control in neuron models. *BioSystems* **67**, 147–156 (2002).
89. Silver, R. A., Traynelis, S. F. & Cull-Candy, S. G. Rapid-time-course miniature and evoked excitatory currents at cerebellar synapses *in situ*. *Nature* **355**, 163–166 (1992).
90. Cathala, L., Brickley, S., Cull-Candy, S. & Farrant, M. Maturation of EPSCs and intrinsic membrane properties enhances precision at a cerebellar synapse. *J. Neurosci.* **23**, 6074–6085 (2003).
91. Rice, S. O. in *Selected Papers on Noise and Stochastic Processes* (ed. Wax, N.) 113–150 (Dover, New York, 1954).
92. Ayaz, A. & Chance, F. S. Gain modulation of neuronal responses by subtractive and divisive mechanisms of inhibition. *J. Neurophysiol.* **101**, 958–968 (2009).
93. Murphy, B. K. & Miller, K. D. Multiplicative gain changes are induced by excitation or inhibition alone. *J. Neurosci.* **23**, 10040–10051 (2003).
94. Finn, I. M., Priebe, N. J. & Ferster, D. The emergence of contrast-invariant orientation tuning in simple cells of cat visual cortex. *Neuron* **54**, 137–152 (2007).
95. Carandini, M. Melting the iceberg: contrast invariance in visual cortex. *Neuron* **54**, 11–13 (2007).
96. Banitt, Y., Martin, K. A. & Segev, I. A biologically realistic model of contrast invariant orientation tuning by thalamocortical synaptic depression. *J. Neurosci.* **27**, 10230–10239 (2007).
97. Cardin, J. A., Palmer, L. A. & Contreras, D. Cellular mechanisms underlying stimulus-dependent gain modulation in primary visual cortex neurons *in vivo*. *Neuron* **59**, 150–160 (2008).
An *in vivo* study of neural gain that involved intracellular recordings from single neurons in primary visual cortex. Stimuli that evoked sustained changes in the resting membrane potential, input resistance and membrane fluctuations modulated the gain of the firing rate–current relationship.
98. Gabbiani, F., Krapp, H. G., Koch, C. & Laurent, G. Multiplicative computation in a visual neuron sensitive to looming. *Nature* **420**, 320–324 (2002).
99. Dittman, J. S., Kreitzer, A. C. & Regehr, W. G. Interplay between facilitation, depression, and residual calcium at three presynaptic terminals. *J. Neurosci.* **20**, 1374–1385 (2000).
100. Eccles, J. C., Katz, B. & Kuffler, S. W. Nature of the 'endplate potential' in curarized muscle. *J. Neurophysiol.* **4**, 362–387 (1941).
101. Feng, T. P. The changes in the end-plate potential during and after prolonged stimulation. *Chin. J. Physiol.* **16**, 341–372 (1941).
102. Betz, W. J. Depression of transmitter release at the neuromuscular junction of the frog. *J. Physiol.* **206**, 629–644 (1970).
103. Elmqvist, D. & Quastel, D. M. A quantitative study of end-plate potentials in isolated human muscle. *J. Physiol.* **178**, 505–529 (1965).
104. Saviane, C. & Silver, R. A. Fast vesicle reloading and a large pool sustain high bandwidth transmission at a central synapse. *Nature* **439**, 983–987 (2006).
105. Trussell, L. O. & Fischbach, G. D. Glutamate receptor desensitization and its role in synaptic transmission. *Neuron* **3**, 209–218 (1989).
106. Abbott, L. F. & Regehr, W. G. Synaptic computation. *Nature* **431**, 796–803 (2004).
107. Abbott, L. F., Varela, J. A., Sen, K. & Nelson, S. B. Synaptic depression and cortical gain control. *Science* **275**, 220–224 (1997).
108. Tsodyks, M. V. & Markram, H. The neural code between neocortical pyramidal neurons depends on neurotransmitter release probability. *Proc. Natl Acad. Sci. USA* **94**, 719–723 (1997); erratum in **94**, 5495 (1997).
109. Carandini, M., Heeger, D. J. & Senn, W. A synaptic explanation of suppression in visual cortex. *J. Neurosci.* **22**, 10053–10065 (2002).
110. Rothman, J. S., Cathala, L., Steuber, V. & Silver, R. A. Synaptic depression enables neuronal gain control. *Nature* **457**, 1015–1018 (2009).
A combined experimental and theoretical study showing that short-term synaptic depression in the excitatory input can convert inhibition-mediated additive shifts in the I–O relationship into multiplicative gain changes.
111. Rancz, E. A. *et al.* High-fidelity transmission of sensory information by single cerebellar mossy fibre boutons. *Nature* **450**, 1245–1248 (2007).
112. Cash, S. & Yuste, R. Linear summation of excitatory inputs by CA1 pyramidal neurons. *Neuron* **22**, 383–394 (1999).
113. Cash, S. & Yuste, R. Input summation by cultured pyramidal neurons is linear and position-independent. *J. Neurosci.* **18**, 10–15 (1998).
114. Tamas, G., Szabadics, J. & Somogyi, P. Cell type- and subcellular position-dependent summation of unitary postsynaptic potentials in neocortical neurons. *J. Neurosci.* **22**, 740–747 (2002).
115. Bernander, Ö., Koch, C. & Douglas, R. J. Amplification and linearization of distal synaptic input to cortical pyramidal cells. *J. Neurophysiol.* **72**, 2743–2753 (1994).
116. Gasparini, S. & Magee, J. C. State-dependent dendritic computation in hippocampal CA1 pyramidal neurons. *J. Neurosci.* **26**, 2088–2100 (2006).
117. Williams, S. R. & Stuart, G. J. Dependence of EPSP efficacy on synapse location in neocortical pyramidal neurons. *Science* **295**, 1907–1910 (2002).
An experimental study of neocortical pyramidal cells showing spatial dependence of synaptic efficacy and that synaptic inputs on the distal dendrites have a much narrower time-window for integration than those at the soma.
118. Williams, S. R. & Atkinson, S. E. Pathway-specific use-dependent dynamics of excitatory synaptic transmission in rat intracortical circuits. *J. Physiol.* **585**, 759–777 (2007).
119. Markram, H. & Tsodyks, M. Redistribution of synaptic efficacy between neocortical pyramidal neurons. *Nature* **382**, 807–810 (1996).
120. Sjostrom, P. J., Turrigiano, G. G. & Nelson, S. B. Neocortical LTD via coincident activation of presynaptic NMDA and cannabinoid receptors. *Neuron* **39**, 641–654 (2003).
121. London, M. & Hausser, M. Dendritic computation. *Annu. Rev. Neurosci.* **28**, 503–532 (2005).
122. Mel, B. in *Dendrites* (eds Stuart, G. J., Spruston, N. & Hausser, M.) 271–284 (Oxford Univ. Press, 2008).
123. Larkum, M. E. & Nevian, T. Synaptic clustering by dendritic signalling mechanisms. *Curr. Opin. Neurobiol.* **18**, 321–331 (2008).
124. Spruston, N. Pyramidal neurons: dendritic structure and synaptic integration. *Nature Rev. Neurosci.* **9**, 206–221 (2008).
125. Sjöström, P. J., Rancz, E. A., Roth, A. & Häusser, M. Dendritic excitability and synaptic plasticity. *Physiol. Rev.* **88**, 769–840 (2008).
126. Stuart, G., Spruston, N. & Häusser, M. (eds). *Dendrites* (Oxford Univ. Press, Oxford, 2008).
127. Nevian, T., Larkum, M. E., Polsky, A. & Schiller, J. Properties of basal dendrites of layer 5 pyramidal neurons: a direct patch-clamp recording study. *Nature Neurosci.* **10**, 206–214 (2007).
128. Hoffman, D. A., Magee, J. C., Colbert, C. M. & Johnston, D. K^+ channel regulation of signal propagation in dendrites of hippocampal pyramidal neurons. *Nature* **387**, 869–875 (1997).
129. Golding, N. L. & Spruston, N. Dendritic sodium spikes are variable triggers of axonal action potentials in hippocampal CA1 pyramidal neurons. *Neuron* **21**, 1189–1200 (1998).
130. Araya, R., Eisenthal, K. B. & Yuste, R. Dendritic spines linearize the summation of excitatory potentials. *Proc. Natl Acad. Sci. USA* **103**, 18799–18804 (2006).
131. Araya, R., Jiang, J., Eisenthal, K. B. & Yuste, R. The spine neck filters membrane potentials. *Proc. Natl Acad. Sci. USA* **103**, 17961–17966 (2006).
132. Palmer, L. M. & Stuart, G. J. Membrane potential changes in dendritic spines during action potentials and synaptic input. *J. Neurosci.* **29**, 6897–6903 (2009).
133. Capaday, C. & van Vreeswijk, C. Direct control of firing rate gain by dendritic shunting inhibition. *J. Integr. Neurosci.* **5**, 199–222 (2006).
134. Spruston, N., Jaffe, D. B., Williams, S. H. & Johnston, D. Voltage- and space-clamp errors associated with the measurement of electrotonically remote synaptic events. *J. Neurophysiol.* **70**, 781–802 (1993).
135. Oviedo, H. & Reyes, A. D. Boosting of neuronal firing evoked with asynchronous and synchronous inputs to the dendrite. *Nature Neurosci.* **5**, 261–266 (2002).
136. Larkum, M. E., Nevian, T., Sandler, M., Polsky, A. & Schiller, J. Synaptic integration in tuft dendrites of layer 5 pyramidal neurons: a new unifying principle. *Science* **325**, 756–760 (2009).
An experimental study that unifies previous work by the same authors by showing that synaptic integration occurs in the thin basal and apical dendrites of L5 pyramidal cells through NMDA receptors. These local nonlinear integration sites can trigger either a regenerative Ca^{2+} spike in the main dendrite or a sodium spike at the soma.
137. Schwindt, P. C. & Crill, W. E. Amplification of synaptic current by persistent sodium conductance in apical dendrite of neocortical neurons. *J. Neurophysiol.* **74**, 2220–2224 (1995).
138. Oviedo, H. & Reyes, A. D. Variation of input–output properties along the somatodendritic axis of pyramidal neurons. *J. Neurosci.* **25**, 4985–4995 (2005).
139. Cook, E. P. & Johnston, D. Voltage-dependent properties of dendrites that eliminate location-dependent variability of synaptic input. *J. Neurophysiol.* **81**, 535–543 (1999).
140. Schwindt, P. C. & Crill, W. E. Synaptically evoked dendritic action potentials in rat neocortical pyramidal neurons. *J. Neurophysiol.* **79**, 2432–2446 (1998).

141. Larkum, M. E., Zhu, J. J. & Sakmann, B. A new cellular mechanism for coupling inputs arriving at different cortical layers. *Nature* **398**, 338–341 (1999).
142. Wei, D. S. *et al.* Compartmentalized and binary behavior of terminal dendrites in hippocampal pyramidal neurons. *Science* **293**, 2272–2275 (2001).
143. Larkum, M. E., Senn, W. & Luscher, H. R. Top-down dendritic input increases the gain of layer 5 pyramidal neurons. *Cereb. Cortex* **14**, 1059–1070 (2004).
144. Vervaeke, K., Hu, H., Graham, L. J. & Storm, J. F. Contrasting effects of the persistent Na^+ current on neuronal excitability and spike timing. *Neuron* **49**, 257–270 (2006).
145. Mehaffey, W. H., Doiron, B., Maler, L. & Turner, R. W. Deterministic multiplicative gain control with active dendrites. *J. Neurosci.* **25**, 9968–9977 (2005).
This experimental and theoretical study shows how Na^+ channels on pyramidal cell dendrites in electric fish confer spatial dependence to the arithmetic operations performed by inhibition during sustained firing.
146. Smith, M. R., Nelson, A. B. & Du Lac, S. Regulation of firing response gain by calcium-dependent mechanisms in vestibular nucleus neurons. *J. Neurophysiol.* **87**, 2031–2042 (2002).
147. Stuart, G., Schiller, J. & Sakmann, B. Action potential initiation and propagation in rat neocortical pyramidal neurons. *J. Physiol.* **505**, 617–632 (1997).
148. Turner, R. W., Meyers, D. E. & Barker, J. L. Localization of tetrodotoxin-sensitive field potentials of CA1 pyramidal cells in the rat hippocampus. *J. Neurophysiol.* **62**, 1375–1387 (1989).
149. Losonczy, A., Makara, J. K. & Magee, J. C. Compartmentalized dendritic plasticity and input feature storage in neurons. *Nature* **452**, 436–441 (2008).
150. Gasparini, S., Migliore, M. & Magee, J. C. On the initiation and propagation of dendritic spikes in CA1 pyramidal neurons. *J. Neurosci.* **24**, 11046–11056 (2004).
151. Losonczy, A. & Magee, J. C. Integrative properties of radial oblique dendrites in hippocampal CA1 pyramidal neurons. *Neuron* **50**, 291–307 (2006).
An experimental study that used glutamate uncaging to show that coincident input onto radial oblique dendrites of CA1 pyramidal cells can trigger a local supralinear Na^+ spike, suggesting that these dendritic compartments can operate as independent computational units.
152. Remy, S., Csicsvari, J. & Beck, H. Activity-dependent control of neuronal output by local and global dendritic spike attenuation. *Neuron* **61**, 906–916 (2009).
153. Ariav, G., Polsky, A. & Schiller, J. Submillisecond precision of the input-output transformation function mediated by fast sodium dendritic spikes in basal dendrites of CA1 pyramidal neurons. *J. Neurosci.* **23**, 7750–7758 (2003).
154. Softky, W. Sub-millisecond coincidence detection in active dendritic trees. *Neuroscience* **58**, 13–41 (1994).
155. Poirazi, P. & Mel, B. W. Impact of active dendrites and structural plasticity on the memory capacity of neural tissue. *Neuron* **29**, 779–796 (2001).
156. Polsky, A., Mel, B. W. & Schiller, J. Computational subunits in thin dendrites of pyramidal cells. *Nature Neurosci.* **7**, 621–627 (2004).
157. Poirazi, P., Brannon, T. & Mel, B. W. Pyramidal neuron as two-layer neural network. *Neuron* **37**, 989–999 (2003).
This theoretical study proposes the idea that local nonlinear dendritic integration enables an individual pyramidal cell to behave like a two-layer network, thereby substantially enhancing its computational power.
158. Nowak, L. P., Bregestovski, P., Ascher, P., Herbert, A. & Prochiantz, A. Magnesium gates glutamate-activated channels in mouse central neurones. *Nature* **307**, 462–465 (1984).
159. Schiller, J., Major, G., Koester, H. J. & Schiller, Y. NMDA spikes in basal dendrites of cortical pyramidal neurons. *Nature* **404**, 285–289 (2000).
160. Major, G., Polsky, A., Denk, W., Schiller, J. & Tank, D. W. Spatiotemporally graded NMDA spike/plateau potentials in basal dendrites of neocortical pyramidal neurons. *J. Neurophysiol.* **99**, 2584–2601 (2008).
161. Rhodes, P. The properties and implications of NMDA spikes in neocortical pyramidal cells. *J. Neurosci.* **26**, 6704–6715 (2006).
162. Theunissen, F. E. From synchrony to sparseness. *Trends Neurosci.* **26**, 61–64 (2003).
163. Jia, H., Rochefort, N. L., Chen, X. & Konnerth, A. Dendritic organization of sensory input to cortical neurons *in vivo*. *Nature* **464**, 1307–1312 (2010).
164. Rancz, E. A. & Hausser, M. Dendritic calcium spikes are tunable triggers of cannabinoid release and short-term synaptic plasticity in cerebellar Purkinje neurons. *J. Neurosci.* **26**, 5428–5437 (2006).
165. Bollmann, J. H. & Engert, F. Subcellular topography of visually driven dendritic activity in the vertebrate visual system. *Neuron* **61**, 895–905 (2009).
166. Waters, J., Larkum, M., Sakmann, B. & Helmchen, F. Supralinear Ca^{2+} influx into dendritic tufts of layer 2/3 neocortical pyramidal neurons *in vitro* and *in vivo*. *J. Neurosci.* **23**, 8558–8567 (2003).
167. Chklovskii, D. B., Mel, B. W. & Svoboda, K. Cortical rewiring and information storage. *Nature* **431**, 782–788 (2004).
168. Pocock, G. & Richards, C. D. Excitatory and inhibitory synaptic mechanisms in anaesthesia. *Br. J. Anaesth.* **71**, 134–147 (1993).
169. Lee, A. K., Manns, I. D., Sakmann, B. & Brecht, M. Whole-cell recordings in freely moving rats. *Neuron* **51**, 399–407 (2006).
170. Dombeck, D. A., Khabbaz, A. N., Collman, F., Adelman, T. L. & Tank, D. W. Imaging large-scale neural activity with cellular resolution in awake, mobile mice. *Neuron* **56**, 43–57 (2007).
171. Wickersham, I. R. *et al.* Monosynaptic restriction of transsynaptic tracing from single, genetically targeted neurons. *Neuron* **53**, 639–647 (2007).
172. Gleeson, P., Steuber, V. & Silver, R. A. neuroConstruct: a tool for modeling networks of neurons in 3D space. *Neuron* **54**, 219–235 (2007).
173. Harsch, A. & Robinson, H. P. Postsynaptic variability of firing in rat cortical neurons: the roles of input synchronization and synaptic NMDA receptor conductance. *J. Neurosci.* **20**, 6181–6192 (2000).
174. Fino, E. *et al.* RuBi-glutamate: two-photon and visible-light photoactivation of neurons and dendritic spines. *Front. Neural Circuits* **3**, 2 (2009).
175. Kiskin, N. I., Chillingworth, R., McCray, J. A., Piston, D. & Ogden, D. The efficiency of two-photon photolysis of a 'caged' fluorophore, o-1-(2-nitrophenyl) ethylpyranine, in relation to photodamage of synaptic terminals. *Eur. Biophys. J.* **30**, 588–604 (2002).
176. Kantevari, S., Matsuzaki, M., Kanemoto, Y., Kasai, H. & Ellis-Davies, G. C. Two-color, two-photon uncaging of glutamate and GABA. *Nature Methods* **7**, 123–125 (2010).
177. Zhang, F., Aravanis, A. M., Adamantidis, A., de Lecea, L. & Deisseroth, K. Circuit-breakers: optical technologies for probing neural signals and systems. *Nature Rev. Neurosci.* **8**, 577–581 (2007).
178. Kole, M. H. *et al.* Action potential generation requires a high sodium channel density in the axon initial segment. *Nature Neurosci.* **11**, 178–186 (2008).
179. Hines, M. L. & Carnevale, N. T. The NEURON simulation environment. *Neural Comput.* **9**, 1179–1209 (1997).

Acknowledgements
I would like to thank D. Attwell, G. Billings, T. Branco, M. Carandini, E. Chaigneau, T. Fernandez-Alfonso, M. Farrant, T. Margrie, A. Roth, J. Rothman, D. Ruedt, J. Sjöström, V. Steuber, K. Vervaeke and D. Ward for comments on the manuscript and J. Rothman and M. Farinella for help with preparing figures. This work was funded by the Medical Research Council, the Biotechnology and Biological Sciences Research Council, and the Wellcome Trust. R.A.S. holds a Wellcome Trust senior research fellowship in basic biomedical science.

Competing interests statement
The author declares no competing financial interests.

FURTHER INFORMATION
Author's UCL homepage http://ucl.ac.uk/npp/as.html
ModelDB: http://senselab.med.yale.edu/ModelDb
neuroConstruct: http://www.NeuroConstruct.org
Neuromatic (electrophysiology acquisition and analysis software): http://www.neuromatic.thinkrandom.com
NeuroML (simulator independent language for defining biologically detailed neuronal and network models): http://www.NeuroML.org
NEURON simulation environment: http://www.neuron.yale.edu

SUPPLEMENTARY INFORMATION
See online article: S1 (box)

ALL LINKS ARE ACTIVE IN THE ONLINE PDF